Received: 29 December 2019 | Revised: 27 May 2020 | Accepted: 29 June 2020 | Published on: 18 August 2020

DOI: 10.1002/joc.6735

RESEARCH ARTICLE

International Journal of Climatology RMetS

Key statistical characteristics of the mesoscale convective systems generated over the Tibetan Plateau and their relationship to precipitation and southwest vortices

Zi Mai[1] | Shen-Ming Fu[2,3] | Jian-Hua Sun[3,4,5] | Liang Hu[6] | Xiu-ming Wang[7]

[1]National Meteorological Center, China Meteorological Administration, Beijing, China

[2]International Center for Climate and Environment Sciences, Institute of Atmospheric Physics, Chinese Academy of Sciences, Beijing, China

[3]University of Chinese Academy of Sciencesn, Beijing, China

[4]Laboratory of Cloud–Precipitation Physics and Severe Storms, Institute of Atmospheric Physics, Chinese Academy of Sciences, Beijing, China

[5]Southern Marine Science and Engineering Guangdong Laboratory, Zhuhai, China

[6]State Key Laboratory of Severe Weather, Chinese Academy of Meteorological Sciences, Beijing, China

[7]China Meteorological Administration Training Center, Beijing, China

Correspondence
Shen-Ming Fu, International Center for Climate and Environment Sciences, Institute of Atmospheric Physics, Chinese Academy of Sciences, Beijing 100029, China.
Email: fusm@mail.iap.ac.cn

Funding information
The authors thank the NCEP, CMA, and JMA for providing the data. Sincere thanks are also extended to Dr. Jun Li for his automatic tracking algorithm. This research was supported by the National Key R&D Program of China (2018YFC1507200), the Strategic Priority Research Program of the Chinese Academy of Sciences (XDA23090101), the National Natural Science Foundation of China (41775046, 91637211, 41675045), and the Youth Innovation Promotion Association of the Chinese Academy of Sciences.

Abstract

Based on hourly geostationary satellite temperature-of-black-body data, 9,754 mesoscale convective systems (MCSs) are found to form over the Tibetan Plateau (TP) during 16 warm seasons. In the whole study period, neither the occurrence numbers of these MCSs nor their other key characteristics are found to have a significant trend of increasing/decreasing. The MCSs can form anywhere over the TP, and ~6.6% of them can move eastward and vacate the TP (defined as the eastward-moving type [EMT]). The EMTs' mean occurrence frequency and lifespan are ~0.3 per day and ~12.0 hr, respectively. Compared to the MCSs that do not vacate the TP, the EMTs usually have stronger intensity, longer lifespan, and develop more rapidly but generate in a drier environment. The vacating stage of an EMT usually begins in the latter half of its lifespan, and an EMT tends to reach its maximum cloud area when it is about to vacate the TP. After vacating the TP, an EMT usually weakens at first and then enhances again. Vorticity budget indicates that the convergence-related horizontal shrinking and the convection-related vertical vorticity transport govern the cyclonic-vorticity increase/maintenance associated with the longer-lived EMTs. Of all the EMTs, only ~8% are associated with southwest vortices (SWVs), and the precipitation related to these EMTs contributes ~20% to the local hourly heavy precipitation. Compared to the EMTs that are not related to SWVs, those that are generally vacate the TP sooner, last longer having vacated the TP, and have longer whole lifespans.

KEYWORDS

application/context, atmosphere, climate, convection, dynamic/processes, geographic/climatic zone, geophysical sphere, mesoscale convective system, mid-latitude, physical phenomenon, scale, synoptic, Tibetan Plateau, tools and methods

1 | INTRODUCTION

Often referred to as the "third pole" of the world, the Tibetan Plateau (TP) is known for its high altitude, large area, and complicated terrain. The dynamical and thermos-dynamical effects associated with these geographical features are remarkable and impact hugely the atmospheric circulation around the TP and even worldwide (Ye and Gao, 1979; Zhao *et al*., 2018). In warm seasons (May–September), the TP acts as a heating source and contributes to the highly frequent occurrences of mesoscale convective systems (MCSs) on the TP (Ye and Gao, 1979; Yang *et al*., 1992; Wang *et al*., 1993). These MCSs play an important role in precipitation over the TP and its downstream regions (Fu *et al*., 2010; Hu *et al*., 2016).

Due to the importance of the MCSs over the TP, much efforts have been made in this field for decades. For instance, the formation and development processes of MCSs over the TP were investigated by Jiang *et al*. (1996) and Chen *et al*. (1999) Their results showed that MCSs' formation was mainly due to the local thermal effect over the TP. Zhu and Chen (1999) suggested that there were two high-frequency centers of MCSs over the TP, one was situated in the southwest TP and the other was located at the northwest TP. Jiang and Fan (2002) found that MCSs over TP could be roughly categorized into three groups: quasi-stationary (accounting for a majority); eastward propagating but not vacating the TP; eastward propagating and vacating the TP (low proportion). Sugimoto and Ueno (2010) pointed out that the southeast-northwest gradation of the soil moisture distribution over the TP could induce MCSs in the eastern TP. Hu *et al*. (2016; 2017) conducted a statistical analysis on the origin, spread, lifespan, precipitation, thermal, and dynamical features of the MCSs over the TP, and compared the similarities and differences between MCSs over the eastern TP and middle TP.

As mentioned above, statistical studies on the MCSs over the TP are an effective way to enhance the understanding of this type of system. All such statistical studies require a dataset that are sufficiently long and reliable. However, compared to many other regions, station observational data are scarce over the TP (Zhao *et al*., 2018) because of its harsh natural conditions. Therefore, satellite observational data may represent the only reliable choice for statistical studies of MCSs over the TP. As a mesoscale process, fine temporal resolution is necessary to identify MCSs accurately. Based on the temporal resolutions of satellite data used to detect MCSs over the TP, previous studies can be classified roughly into three groups: (a) greater than three-hourly, for example, early studies that used data from the Television Infrared Observation Satellite and Nimbus satellites (Flohn and Reiter, 1968; Qian *et al*., 1984); (b) three-hourly (or approximately so), for example, studies that used (1) deep convection data from the International Satellite Cloud Climatology Project (ISCCP) (Li *et al*., 2008), (2) precipitation-features data from the Tropical Rainfall Measuring Mission (TRMM) (Qie *et al*., 2014; Xu and Zipser, 2015), and (3) an improved ISCCP convection tracking database (Hu *et al*., 2016; 2017); (c) hourly, for example, studies that used (1) Japanese Geostationary Meteorological Satellite data (Jiang *et al*., 1996; Jiang and Fan, 2002), (2) Meteosat-5 data (Sugimoto and Ueno, 2010), and (3) Chinese Fengyun-2C data (Fu *et al*., 2011).

Compared to the satellite data used in groups (a) and (b), the hourly data in group (c) are more reliable for tracking MCSs generated over the TP. However, related studies to date have focused mainly on relatively short study periods (i.e., no more than 9 years) (Sugimoto and Ueno, 2010) and rarely include analyses of satellite data later than 2006. Even for studies in groups (a) and (b), satellite data later than 2011 are rarely used. Therefore, to understand MCSs over the TP more comprehensively, it is necessary to focus on a longer study period and include new satellite observations in the analysis.

As documented in previous studies (Jiang and Fan, 2002; Fu *et al*., 2011; Hu *et al*., 2016), the MCSs generated over the TP can be classified roughly into two types: (a) those that move eastward and vacate the TP (referred to hereinafter as the eastward-moving type [EMT]) and (b) those that either do not move eastward or do so but dissipate over the TP (referred to hereinafter as the non-eastward-moving/dissipating type [NDT]). The differences between EMTs and NDTs have been addressed in related studies (Chen *et al*., 1999; Zhuo *et al*., 2002; Dai *et al*., 2007; Fu *et al*., 2011; Zhao *et al*., 2018). Nevertheless, some key features of these two types remain rarely discussed. The EMTs show distinct features related to whether they are over the TP or have vacated it. Having vacated the TP, some EMTs last for relatively shorter times whereas others can last longer and exert more influence on downstream regions. The outstanding questions are (a) How do the key features of an MCS change upon vacating the TP? (b) What are the main differences between longer- and shorter-lived EMTs? (c) Which factors govern the evolution of longer-lived EMTs? In addition, some EMTs can induce southwest vortices (SWVs) upon vacating the TP (Zhao *et al*., 2004; Fu *et al*., 2010; Fu *et al*., 2019). However, the statistical relationship between SWVs and EMTs remains to be determined.

As mentioned above, the main aims of the present study are (a) to supplement the statistical understanding of MCSs over the TP by analysing hourly satellite data

from a longer period that contains more-recent observations, (b) to determine key differences among different types of MCSs and verify the main changes that occur when EMTs vacate the TP, (c) to show the main factors governing the evolution of longer-lived EMTs, and (d) to illustrate the statistical relationship between EMTs and SWVs. Because MCSs over the TP occur most frequently and have strongest intensity in the warm season (May–September) (Hu *et al*., 2016), and their associated torrential precipitation also mainly appears in this period (Zhao *et al*., 2004; Zhao *et al*., 2018), in the present study we focus only on those MCSs generated in warm seasons.

The remainder of this paper is structured as follows. In Section 2 we present our data and methods, and in Section 3 we discuss the key statistical characteristics of MCSs generated over the TP. In Section 4 we analyse the composite features of different types of MCSs, in Section 5 we calculate the contribution of MCS-related precipitation, and in Section 6 we establish the relationship between EMTs and SWVs. Finally, in Section 7 we show the conclusion and discussion.

2 | DATA AND METHODS

2.1 | Data

In the present study, the hourly $0.05^\circ \times 0.05^\circ$ temperature of black body (TBB) data observed by five geostationary satellites (GMS-5, GOES-9, MTSAT-1R, MTSAT-2, Himawari-8) in the infrared range (Table 1) are used to detect and track MCSs generated over the TP during the warm seasons of 2000–2016. This TBB product were provided by Japan Meteorological Agency (JMA) through Kochi University website (http://weather.is.kochi-u.ac.jp/archive-e.html). Table 1 shows the periods and specifications of the satellites used in this study. It should be noted that, although the TBB data are from multiple satellites that used different sensors and/or data processing procedures, the intercalibrations among these satellites in terms of the thermal infrared band (IR1) indicate that the differences of the brightness temperature among these satellites are less than 1 K (Tahara *et al*., 2004; Tahara and Ohkawara, 2005; Murata *et al*., 2015). This means that the errors due to using different sensors and/or data processing procedures can be ignored in this study.

TABLE 1 Periods and specifications used in this study for each of the satellites

Satellite	Period	Infrared wavelength (μm)
GMS-5	May 1, 2000, 00UTC–May 21, 2003 23UTC	11.0
GOES-9	May 22, 2003, 00UTC–Sep 30, 2004 23UTC	10.7
MTSAT-1R	May 1, 2006, 00UTC–Sep 30, 2010 23UTC	10.8
MTSAT-2	May 1, 2011, 00UTC–Jul 1, 2015 23UTC	10.8
Himawari-8	Jul 7, 2015, 00UTC–Sep 30, 2016 23UTC	10.4

To analyse the MCSs' circulations, we use the six-hourly $0.5^\circ \times 0.5^\circ$ Climate Forecast System version 1 (2000–2010) (Saha *et al*., 2006) and version 2 (2011–2016) (Saha *et al*., 2014) Re-analysis data (CFSR) from the National Centers for Environmental Prediction (NCEP). To analyse the local precipitation related to the MCSs, we use the half-hourly $0.0727^\circ \times 0.0727^\circ$ National Oceanic and Atmospheric Administration CPC Morphing Technique (CMORPH) high-resolution precipitation data (Joyce *et al*., 2004) and rain-gauge-based hourly accumulated precipitation data from the China Meteorological Administration (CMA). CMORPH uses precipitation estimates that have been derived from low orbiter satellite microwave observations exclusively. Their features are transported via spatial propagation information that is obtained entirely from the geostationary satellite IR data.

Because the JMA satellite TBB data could be missing or incomplete, we begin by checking the data integrity rate, which is simply calculated by the times of data available to the whole times in each year/month, to ensure reliable statistics. It is found that, except for 2005, during which the data integrity rate is only ~66.1% (not shown), the data integrity rates for the other periods (by year/month) are mostly above 90% (Figure 1). Therefore, the present focus period comprises the 16 warm seasons from 2000 to 2016 excluding 2005.

2.2 | Tracking methods and key parameters

To identify an MCS, one must first specify standards for its area, intensity, and lifespan (Maddox, 1980; Augustine and Howard, 1991). Based on previous studies and the characteristics of MCSs over TP, the following standards are used herein to identify MCSs: (a) the MCSs must form within the region 26–40°N, 75–103°E, where the altitude exceeds 3,000 m (Figure 2); this guarantees that they are generated over the TP. (b) their cloud area with TBB $\leq -52^\circ$C must exceed 5,000 km^2. The TBB standard of $\leq -52^\circ$C is determined following those documented in Zheng *et al*. (2008) and Yang *et al*. (2018), both of which

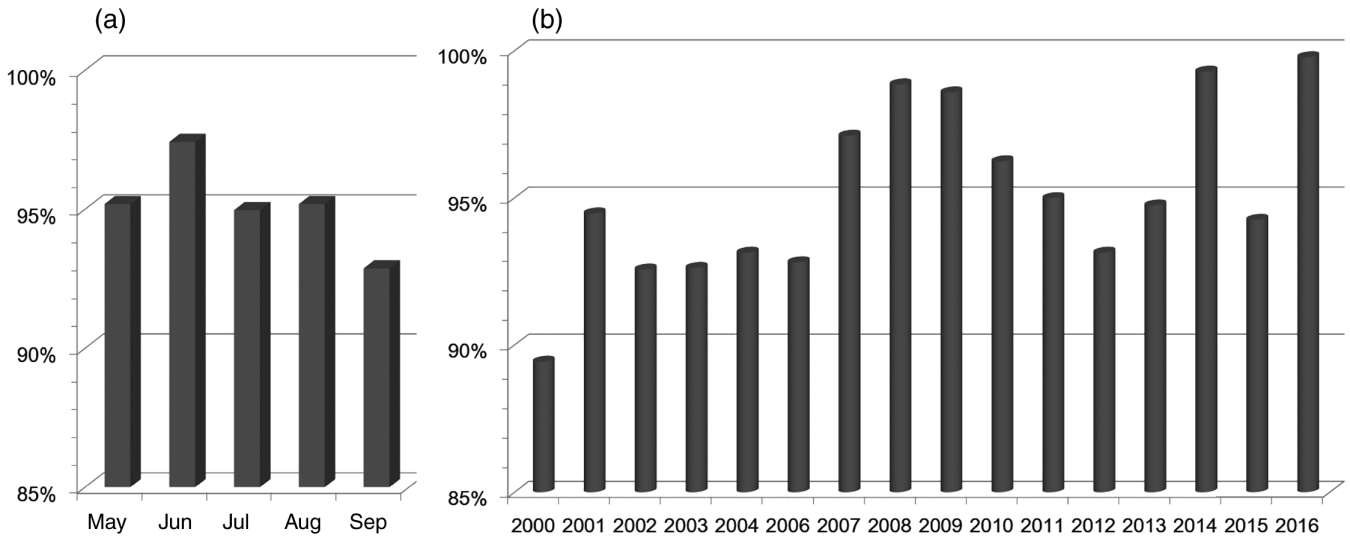

FIGURE 1 Data integrity (units: %): (a) yearly; and (b) monthly

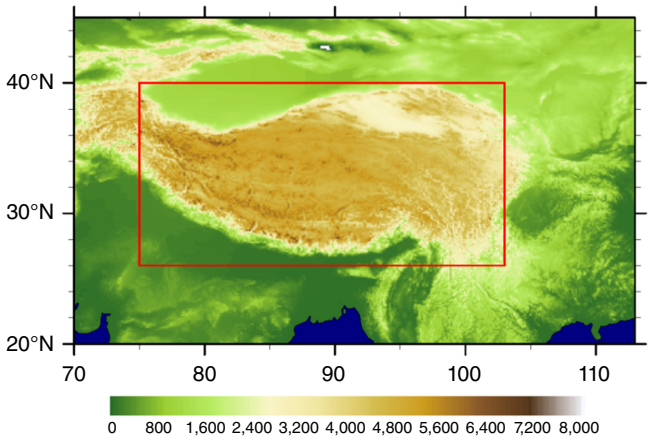

FIGURE 2 Terrain height of the TP (shading, units: m). MCSs generated within the red box (26–40°N, 75–103°E) with a height above 3,000 m are considered to be generated over the TP

point out that this standard is appropriate for identifying MCSs that are generated over the TP and TP's surrounding regions. Moreover, Laing and Fritsch (1997), and Yang *et al*. (2015) also used −52°C as the criterion in their studies. The area standard is determined following Mathon and Laurent (2001), who find that if the lower limit of MCS area is set <5,000 km^2, the number of detected MCSs will increase greatly and thus regenerations of these systems might be missed. In addition, Yang et al. (2018) has confirmed the validation of the area standard (≥5,000 km^2) in regions surrounding the TP. (c) criterion 2 must be satisfied for at least three consecutive hours, since Parker and Johnson (2000) has suggested that an MCS's time scale is f^{-1} (where f is the Coriolis parameter). It is around 3 hr at mid-latitudes.

The time at which an MCS meets condition 2 for the first time is defined as when it forms, and the time at which an MCS either no longer meets condition 2 or merges with a larger MCS is defined as when it dissipates. The period between the formation and dissipation of an MCS is defined as its lifespan. At any given hour, the location of the centroid of an MCS is taken as its position. We define 103°E as the eastern boundary of the TP; if an MCS moves farther east than 103°E then it is deemed to have vacated the TP. Therefore, in the present study, an MCS vacating the TP means simply that it moves farther east than 103°E. Based on the position of an EMT relative to 103°E, its lifespan can be divided into two stages, namely (a) when it is over the TP (before it vacates) and (b) when it is off the TP (after it vacates).

Accurate tracking of MCSs is vital for a statistical study on MCSs such as this work. This will effectively differ the locally generated MCSs from those moving in. To ensure the accuracy of MCS tracking, all the MCSs studied herein were first detected by an automatic tracking algorithm that has been confirmed to be effective (Li, 2010), and then verified manually. For computational efficiency, the tracking range was restricted to 20–45°N, 70–113°E; tracking was stopped if an MCS exited this range. Nevertheless, we found from manual verifications that very few MCSs (∼0.1%) exited this range, making it appropriate for the present study. The automatic tracking algorithm was developed by Li (2010) and involves five main steps:

1. read TBB data at time t, and use the nine-point smoothing method to remove noise interferences;
2. identify MCSs according to the area and intensity standards discussed above and obtain key features of the MCSs at time t;

3. read data at time $t + 1$ and repeat steps (1) and (2);
4. match MCSs detected at times t and $t + 1$;

The following three standards are used to match MCSs: (a) the distance standard—from time t to $t + 1$, the displacement of an MCS's center should be less than 165 km; (b) the R-descriptor standard (Lu *et al*., 1987), which is approximately invariant during translation, rotation, and scaling of an MCS; (c) the Hu-moment standard (Hu, 1962), which is effective for shape recognition.

5. loop steps (1)–(4) until the end of the study period.

Note that although the tracking algorithm performs well in identifying and tracking MCSs, it generates obvious errors when MCSs split or merge, as do many other algorithms. Therefore, it is necessary to verify and correct (where necessary) the detected MCSs manually. Based on the correction methods documented in Mathon and Laurent (2001) and Feng *et al*. (2012), our correction method includes three key points: (a) when two or more MCSs merge together, the merged MCS is assumed to be the continuation of the largest MCS, while the smaller MCSs are terminated; (b) when an MCS splits into several smaller parts, the largest part is assumed to continue tracking as the original system and the smaller parts are assumed as formation of new MCSs if they can satisfy the MCS criterion; (c) the corrected MCSs must satisfy the criterions used in the automatic tracking algorithm. In the present study, all the MCSs detected by the tracking algorithm underwent three rounds of manual verification, thereby ensuring reliability.

2.3 | Standardized time and area growth rate

Because MCSs can have different lifespans, we define the following standardized time (ST) to represent certain stages during MCSs' lifespans by using a percentage and to compare typical stages in the lifespans of different MCSs:

$$\mathrm{ST}=\frac{t_T}{WL}, \tag{1}$$

where t_T is a typical time (e.g., halfway through the lifespan) of an MCS and WL is its lifespan.

In this study, the area growth rate (AGR) of an MCS is defined as

$$\mathrm{AGR}=\frac{S(t)-S(t-1)}{S(t-1)}, \tag{2}$$

where S is the cloud area of the MCS as determined by the tracking algorithm, t is the current time, and $t - 1$ is the previous time.

2.4 | Vorticity budget

As the evolution of an MCS can be effectively reflected by vorticity (Fu *et al*., 2010; 2011), a vorticity budget is used to understand its variation. The equation (Fu *et al*., 2017) is as follow:

$$\frac{\partial\zeta}{\partial t}=\underbrace{-\mathbf{V}_h\cdot\nabla_h\zeta}_{\mathrm{HAV}}\underbrace{-\omega\frac{\partial\zeta}{\partial p}}_{\mathrm{VAV}}+\underbrace{\mathbf{k}\cdot\left(\frac{\partial\mathbf{V}_h}{\partial p}\times\nabla_h\omega\right)}_{\mathrm{TIL}}\underbrace{-\beta v}_{\mathrm{APV}}\underbrace{-(\zeta+f)\nabla_h\cdot\mathbf{V}_h}_{\mathrm{STR}}+\mathrm{RES}, \tag{1}$$

where ζ stands for the relative vorticity, $\mathrm{V}_h = ui + vj$ is the horizontal wind vector, $\nabla_h=\frac{\partial}{\partial x}\mathbf{i}+\frac{\partial}{\partial y}\mathbf{j}$, vectors $(\mathbf{i},\mathbf{j},\mathbf{k})$ are the unit vectors pointing to the east, north, and zenith, respectively, the subscript h represents the horizontal component, p is pressure, f is the Coriolis parameter, $\omega = dp/dt$, and $\beta = \partial f/\partial y$. Terms HAV and VAV denote the horizontal and vertical advection of vorticity, respectively; TIL is tilting; APV represents the advection of planetary vorticity, because this term is much smaller than the other four terms, it is only used in calculating the total effect (TOT); STR is stretching; and RES is the

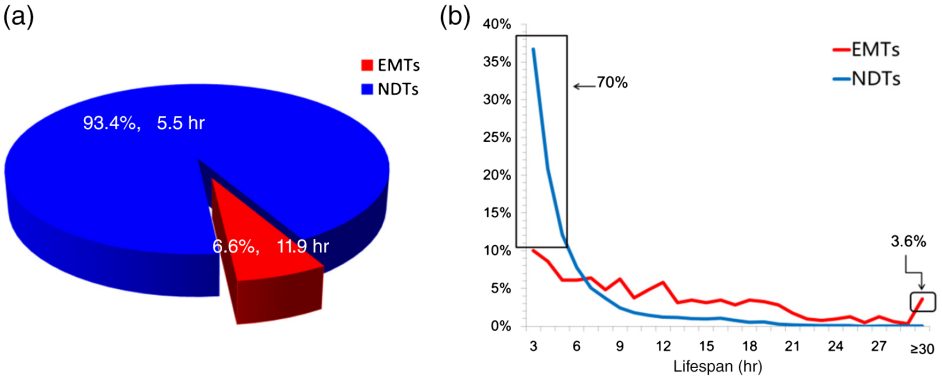

FIGURE 3 Panel (a) shows respective contributions of EMTs and NDTs to the total MCS numbers, as well as their mean lifespans. Panel (b) illustrates contributions of different lifespans to the total EMT and NDT numbers, respectively

residual effect. TOT = HAV + VAV + TIL + APV + STR, which represents the total effect.

3 | STATISTICAL CHARACTERISTICS OF DIFFERENT TYPES OF MCS

3.1 | Occurrence frequency and lifespan

During the 16 warm seasons, 9,754 MCSs were generated over the TP, equivalent to around four MCSs per day. Therefore, MCSs are active over the TP during the warm season. Of these 9,754 MCSs, only around 640 were EMTs (Figure 3a), equivalent to around two EMTs per week; the remaining MCSs (9,114) were all NDTs. Therefore, EMTs do not occur frequently. The mean EMT lifespan is ~12.0 hr, more than twice the NDT one (~6.0 hr), meaning that EMTs generally last much longer than do NDTs.

The distributions of EMT and NDT lifespans are shown in Figure 3b. For both EMTs and NDTs, shorter-lived MCSs are in the majority. Compared to that of NDTs, longer-lived EMTs account for a larger contribution in their total numbers. Only around 25% of all NDTs last longer than 6 hr, whereas around 70% of all EMTs do so. In addition, ~8.4% (resp. ~0.3%) of all EMTs (resp. NDTs) persist for more than 24 hr, while only EMTs (~3.6%) persist for more than 30 hr. Overall, EMTs tend to account for a larger percentage of the total number of MCSs than that of NDTs, as the MCS lifespan increases.

3.2 | Temporal variation features

3.2.1 | Warm-season variations

In each warm season, the MCSs generated over the TP show different features. The maximum number of MCSs formed in a warm season was 798 in 2016 and the minimum was 445 in 2015. During the study period, the mean percentage contribution of EMTs to the total number of MCSs was ~6.6%. However, the annual contribution varies considerably, with a maximum of around 9.8% in 2003 and a minimum of around 4.9% in 2012 (Figure 4c).

The warm-season mean lifespan of the MCSs generated over the TP also exhibits obvious changes during the study period (not shown). For EMTs and NDTs, the maximum warm-season mean lifespans are ~14.0 hr in 2012 and ~6.0 hr in 2014, respectively, and the corresponding minima are ~9.0 hr in 2000 and ~5.0 hr in 2002, respectively.

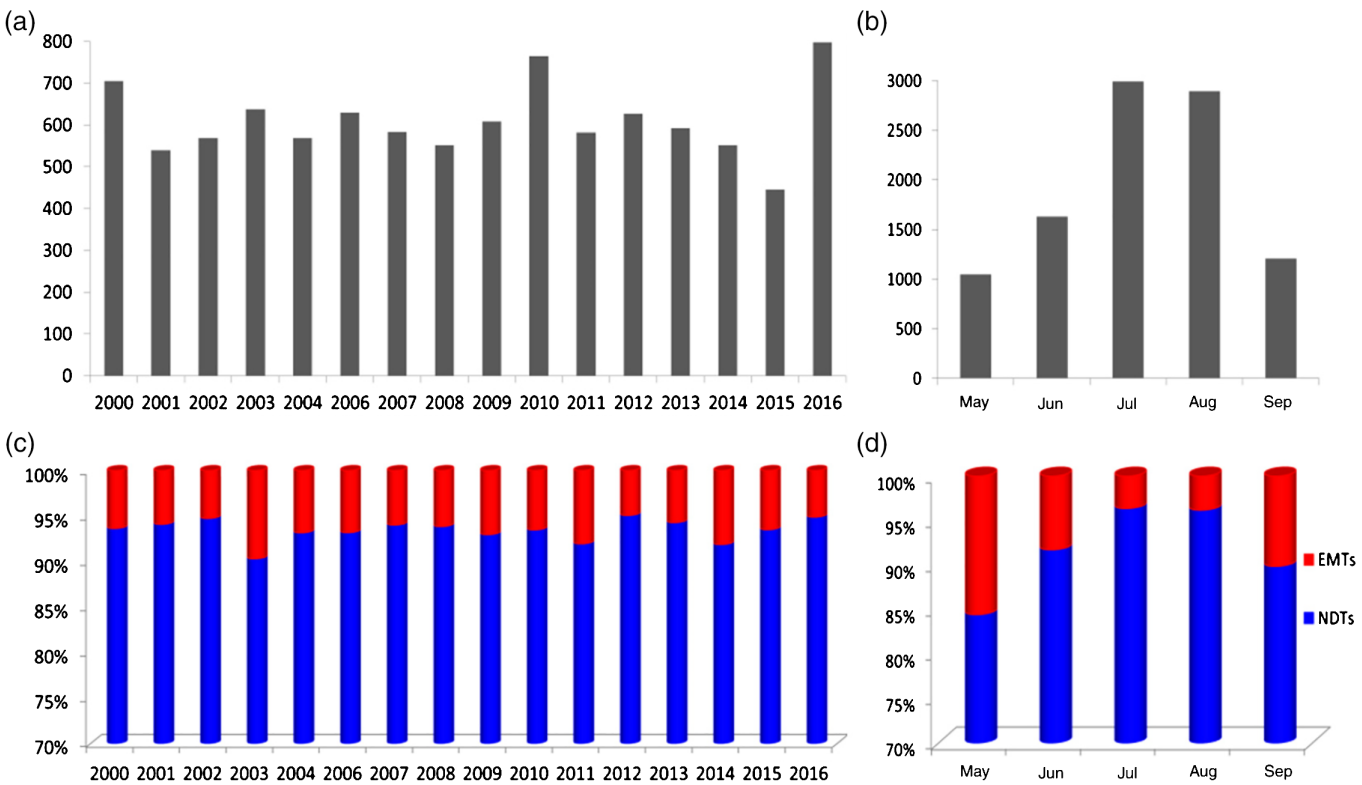

FIGURE 4 Warm-season (a, c) and monthly (b, d) variations of different types of MCSs, where (a–b) are the numbers, and (c–d) are the respective contributions (units: %) of EMTs and NDTs to the total MCS numbers

3.2.2 | Monthly variations

The MCSs generated over the TP feature significant monthly variations (Figure 4b,d). On average, the MCSs generated over the TP in July and August account for more than 60% of the total number of MCSs (Figure 4b), whereas, those that form in May only account for a contribution of ~10.7%. The percentage of EMTs each month shows a trend that is approximately opposite to that of the total number of MCSs each month (see Figure 4b,d). The respective proportions of EMTs in July and August, namely ~3.6 and ~3.8%, are much less than those in the other months, whereas the largest EMT contribution appears in May, namely ~15.6% (Figure 4d). This remarkable monthly variation in EMT contribution is closely related to the enhancement of the West Pacific subtropical high from Spring to Summer, and the variation in latitude of the westerly jet over the TP (Hu *et al.*, 2016), which undergoes two northward shifts during the transition season from winter to summer (Li *et al.*, 2004). The EMTs and NDTs show consistent features in their respective mean lifespans: they both experience maximum monthly mean lifespans in July (~15.0 hr for EMTs and ~6.0 hr for NDTs), followed by August (~13.0 hr for EMTs and ~6.0 hr for NDTs), and they both experience minimum values in May (~9.0 hr for EMTs and ~5.0 hr for NDTs).

According to Kondo *et al.* (2006), heavy precipitation tends to occur when TBB has a large spatial gradient, and the MCSs with larger TBB spatial gradients usually intensify more rapidly. The minimum TBB and the maximum TBB spatial gradient are important characterizations for both convection and precipitation. Therefore, the TBB spatial gradient is calculated as a key factor for the MCS's evolution. Overall, EMTs and NDTs feature similar variation trends in monthly average maximum TBB spatial gradient and monthly average minimum TBB: (a) their monthly average maximum TBB spatial gradients are both minimum in May, grow in June, are maximum in July and August, and decrease in September (Figure 5a); (b) their monthly average minimum TBBs (the MCSs with lower TBB usually have higher height and greater intensity) show opposite trends to those in (a), that is, they are maximum in May, decrease in June, are minimum in July and August, and increase in September (Figure 5c). Thus, it can be concluded that the EMTs and NDTs in July and August usually have the strongest intensities and development the fastest.

Each month, the EMT mean maximum TBB spatial gradient exceeds the NDT one and the EMT mean minimum TBB is lower than the NDT one; these two features mean that EMTs have stronger intensities and develop

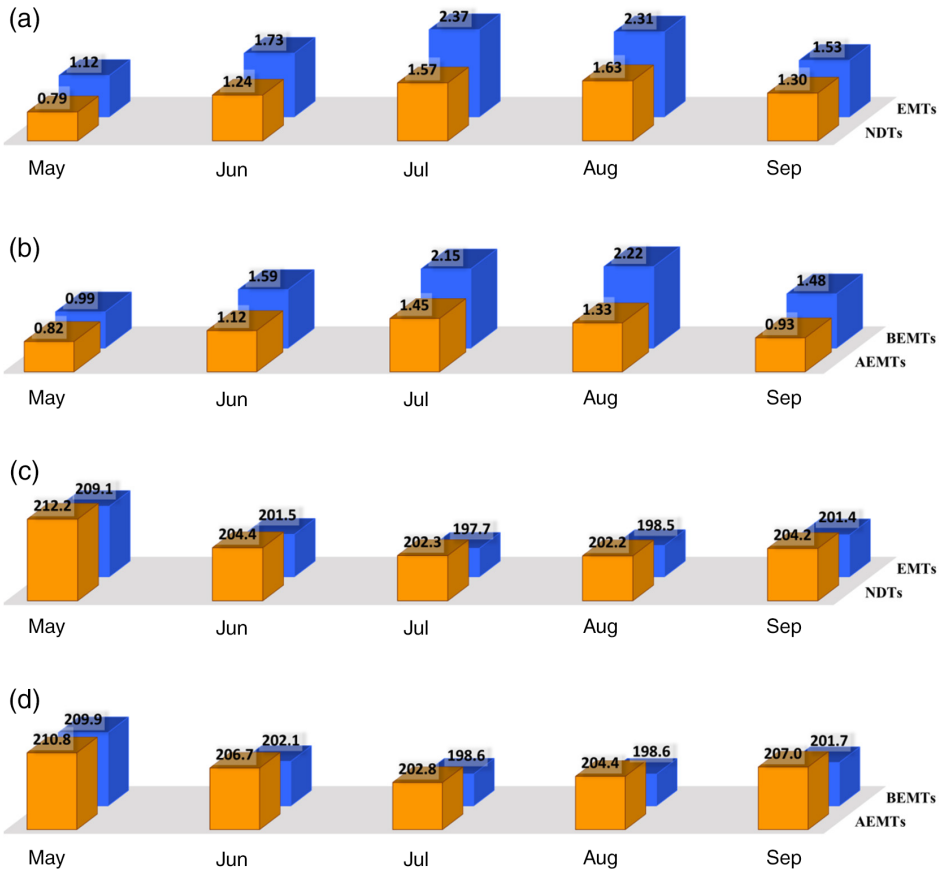

FIGURE 5 Panel (a) shows the monthly mean maximum TBB gradients (units: K km^{-1}) of EMTs (blue) and NDTs (orange). Panel (b) is the same as (a), but for EMTs before (blue) and after (orange) they vacate the TP. Panel (c) illustrates the monthly mean minimum TBB (units: K) of EMTs (blue) and NDTs (orange). Panel (d) is the same as (c), but for EMTs before (blue) and after (orange) they vacate the TP. AEMT, after an EMT move off the TP; BEMT, before an EMT move off the TP

faster. Regardless of whether EMTs are over the TP or have vacated it, the variation trends in their monthly mean maximum TBB spatial gradients and minimum TBBs remain largely unchanged (Figure 5b,d). These variation trends are similar to those of EMTs and NDTs as shown in Figure 5a,c.

3.2.3 | Diurnal variations

As the TP spans more than two time zones, to compare MCSs' generation time in different time zones, we convert UTC to local standard time at a temporal resolution of 0.5 hr, and use the resulting local generation time of each MCS for analysis. Figure 6 shows that the occurrence number of MCSs increases rapidly from 1200 and peaks at 1400–1600 when the maximum surface temperature appears; then the occurrence number decreases until the next day. This is consistent with that reported by Zheng *et al.* (2008).

The EMTs and NDTs have similar diurnal variation trends (Figure 6) but with two obvious differences. First, the maximum number of EMTs occurring happens around 1430, whereas the equivalent time for NDTs is roughly an hour later, meaning that their environmental circulations may show significant differences, as the diurnal variations of solar radiation are similar for EMTs and NDTs. Second, the EMTs generated during the day (0600–2000) account for ~77.5% of all EMTs, with ~56.9% appearing in the afternoon (1200–1700). The equivalent percentages for NDTs are ~66.3 and ~43.2%, respectively, meaning that the formation of EMTs depends more on solar radiation than does that of NDTs.

3.3 | Spatial distribution and tracks

During the warm season, MCSs can form anywhere over the TP, with most of them (~84.4%) dissipating over the TP (Figure 7a–c). By interpolating the hourly-resolution MCS locations (i.e., all positions on their tracks) and their formation locations onto grids of 0.5° × 0.5° spatial resolution, we obtain the spatial frequency distributions of MCS activity (Figure 7d–f) and formation (Figure 8). From Figure 7d, the southern TP clearly features far more MCS activity than does the northern TP. Two maximum centers appear over the southern TP, one located in the southeastern TP and the other in the southwestern TP. These two centers are mainly due to NDTs (Figure 7d,f). The latter center, which has two cores, is slightly stronger than the former center. This is consistent with the findings reported by Jiang and Fan (2002), Hu *et al.* (2017) and other previous works (Sugimoto and Ueno, 2010).

The EMTs and NDTs have significantly different spatial distribution features. EMTs are generated in the middle and eastern sections of the TP (Figure 8a), particularly over the eastern flank of the TP, with a maximum frequency center located around 33°N and 102°E. Correspondingly, EMTs mainly influence regions east of 90°E (Figure 7e), whereas those MCSs that form west of 90°E usually do not vacate the TP. NDTs can form anywhere over the TP and affect everywhere therein (Figures 7f and 8b). Generally, there is more NDT formation and activity over the southern TP than over the northern TP, confirming the results obtained by Hu *et al.* (2016).

The MCSs that dissipate having vacated the TP can vacate the plateau in almost any direction (Figure 7a). Most of those MCSs dissipate soon after vacating the TP, but some continue moving. During the tracking process, we found that very few MCSs (~0.1%) vacated the region 20–45°N, 70–113°E; those that did usually developed again after merging with local MCSs, thereby extending their lifespans. In this study, the direction in which an EMT moves can be classed as one of three according to the position of its start point (i.e., the average location of the MCS during its first 2 hr) relative to its end point (i.e.,

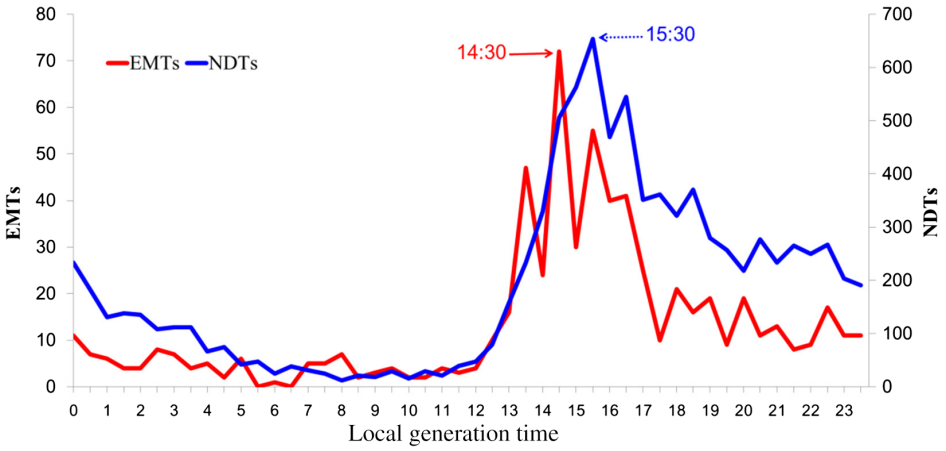

FIGURE 6 Generation times (local standard time) and numbers of EMTs and NDTs

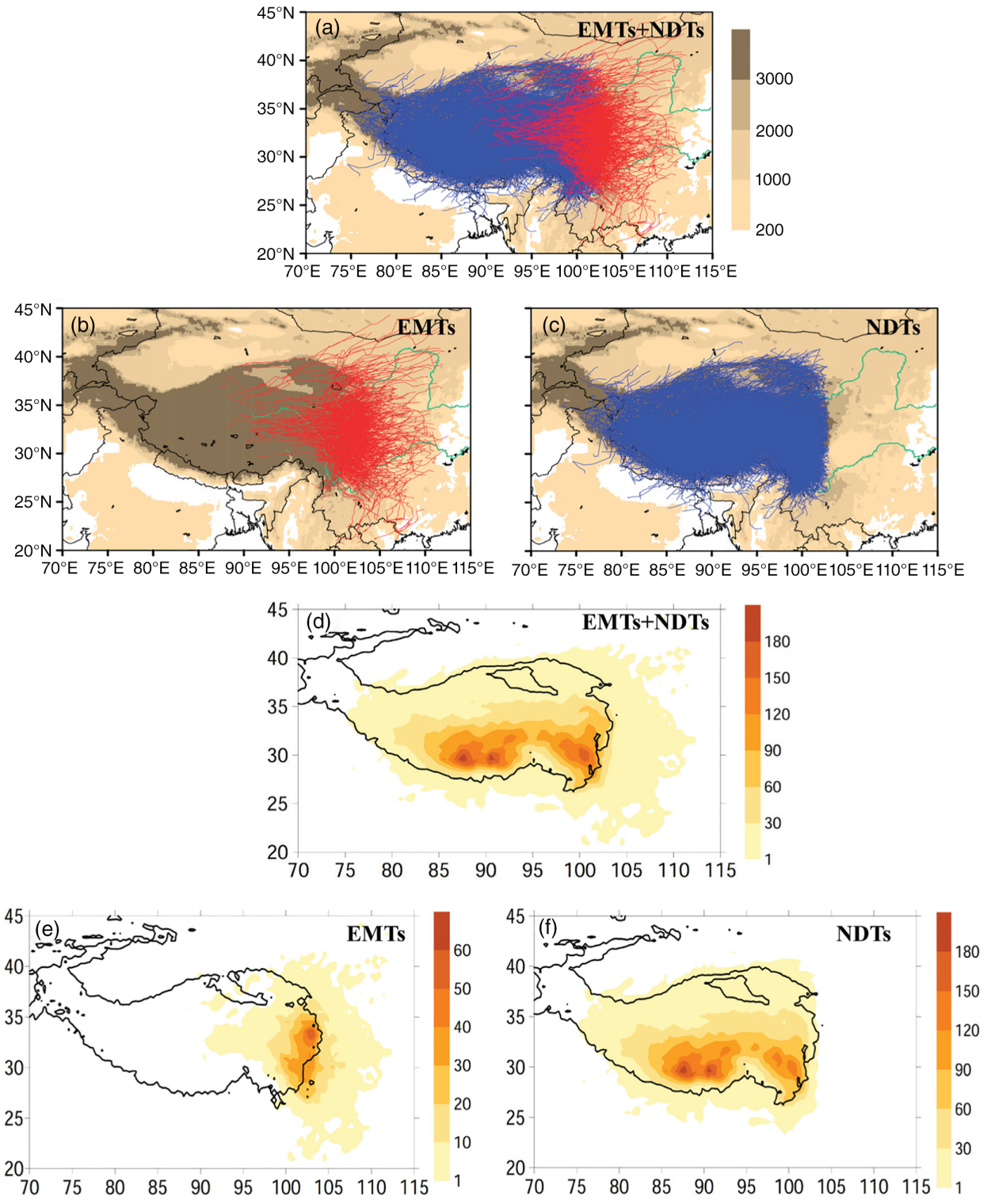

FIGURE 7 Tracks of MCSs generated over the TP (a–c), and the spatial distribution of their frequency (d–f), where shading in (a–c) stands for the terrain, and thick black line in (d–f) outlines the altitude of 3,000 m. Panels (a) and (d) are total MCSs, panels (b) and (e) are EMTs, and panels (c) and (f) are NDTs

the average location of the MCS during its last 2 hr). If the angle between the line linking the start and end points and the latitude line is between ±30°, then the MCS is defined as eastward moving; if the angle is greater than +30°, it is defined as northeastward moving; and if the angle is less than −30°, it is defined as southeastward moving. As Figure 7a–c illustrate, after vacating the TP, EMTs usually move off to the

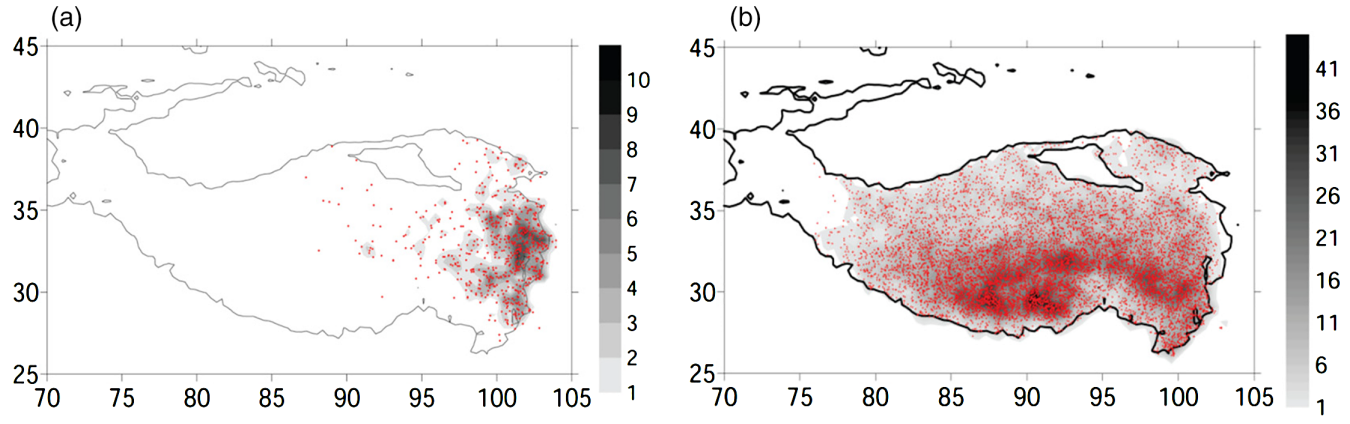

FIGURE 8 Spatial distribution of MCSs' generation locations (red dots) and MCSs' generation numbers (grey shading): (a, c) EMTs; (b, d) NDTs. Black solid line shows the topography height of 3,000 m

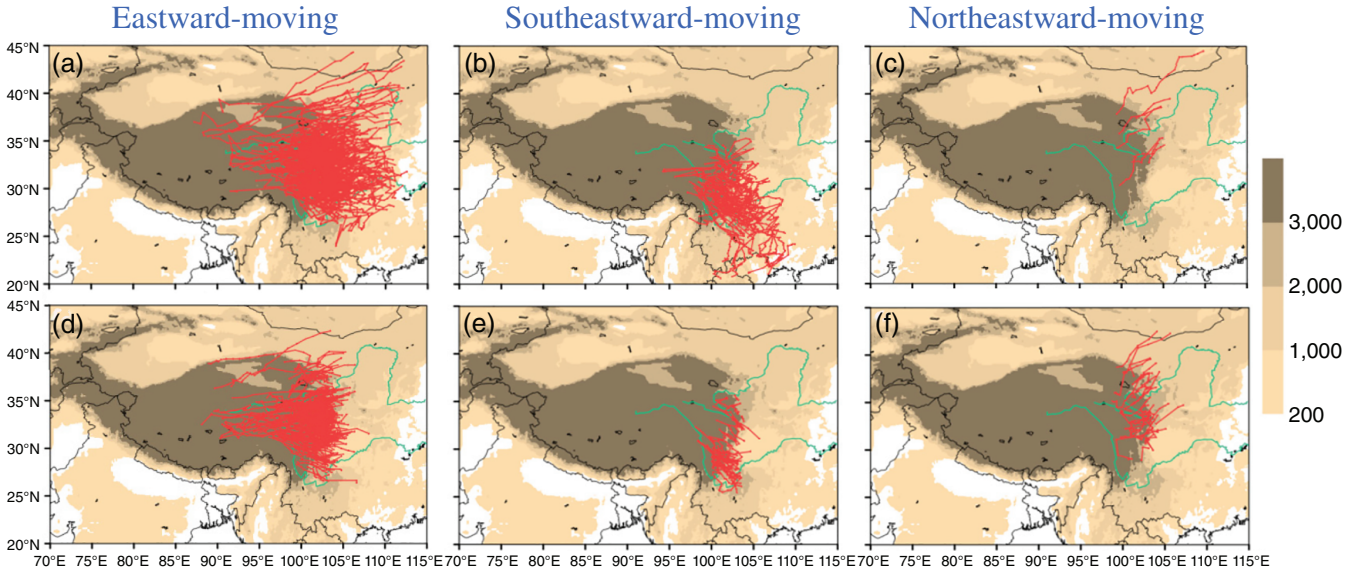

FIGURE 9 Tracks of different types of EMTs: Panels (a–c) show L-EMTs, and panels (d–f) show S-EMTs. The left column is eastward-moving EMTs, the middle column is southeastward-moving EMTs, and the right column is northeastward-moving EMTs. Shading shows the terrain

northeast, east, or southeast. Because the lifespan of an MCS and the time that it survives having vacated the TP may differ remarkably from one MCS to another and because longer-lived MCSs tend to have more significant influences on downstream regions, we classify EMTs further as follows. Those EMTs that last for at least 6 hr and persist for at least 3 hr after vacating the TP are regarded as longer-lived EMTs (L-EMTs). Meanwhile, those EMTs that do not last for 6 hr or that dissipate within 3 hr of vacating the TP are defined as shorter-lived EMTs (S-EMT).

During the study period, the numbers of L-EMTs (314; ~49.1%) and S-EMTs (326; ~50.9%) are very close to each other. Overall, of all the EMTs, ~78.3% move eastward, ~15.1% move southeastward, and only ~6.6% move northeastward (Figure 9). The respective proportions of eastward-moving events in both L- and S-EMTs are almost the same (~78%) (Figure 9a,d). By contrast, events moving in the other two directions account for remarkably different percentages for the L- and S-EMTs. The proportion of southeastward-moving events of L-EMTs is ~19.1%, which is higher than that of the S-EMTs (~11.3%). By contrast, there are more northeastward-moving events (~10.4%) for S-EMTs than for L-EMTs (~2.5%). From the above discussion, we conclude that those EMTs moving southeastward

have the largest probability (~61.9%) of persisting for a longer time after vacating the TP, while EMTs moving northeastward have the largest probability (~81.0%) of dissipating rapidly when they vacate the TP.

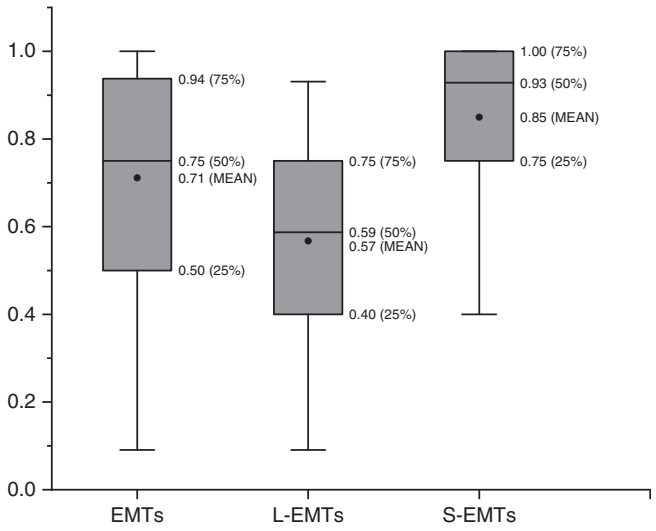

FIGURE 10 Box-and-whisker plots of standardized times of moving-out for (a) EMTs, (b) L-EMTs, and (c) S-EMTs, where MEAN indicates the mean value

3.4 | Typical stages and TBB features

As Figure 10 shows, for all EMTs the average ST when they begin to vacate the TP is 0.71, with a median of 0.75; this means that EMTs generally spend longer over the TP than off it. For L-EMTs, the corresponding average ST is 0.57 and the median is 0.59, both of which mean that L-EMTs generally begin to vacate the TP roughly halfway through their lifespans. By contrast, the average ST for S-EMTs is 0.85 and the median is 0.93; this means that S-EMTs spend much longer over the TP and usually dissipate rapidly after vacating it.

Monthly features of the maximum cloud areas of EMTs and NDTs are shown in Figure 11a. Clearly, EMTs usually have a larger area than do NDTs. Regarding the ratio of MCSs larger than 200,000 km^2, EMTs also have larger proportions, particularly in July and August. The respective maximum cloud areas of an EMT before and after it vacates the TP are shown in Figure 11c, from which it can be seen that in May the respective maximum areas before and after an EMT vacates the TP show no obvious difference. By contrast, from June to September the EMTs usually have larger maximum cloud areas over the TP than those after they vacate it. This indicates that EMTs generally tend to shrink in cloud area after they vacate the TP.

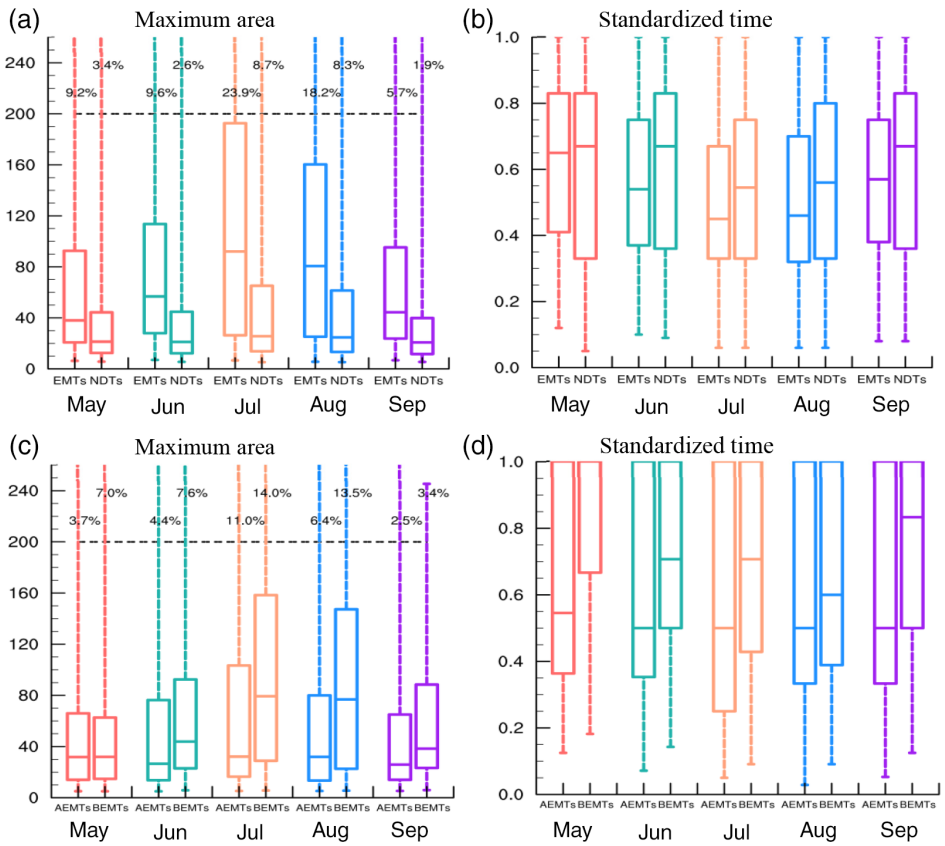

FIGURE 11 Panel (a) is the box-and-whisker plot of maximum cloud areas (units: 10^3 km^2) for EMTs and NDTs, respectively, where cases with a cloud area above 200,000 km^2 are only shown by their percentage. Panel (b) is the box-and-whisker plot of standardized times when the maximum cloud area in panel (a) appear. Panel (c) is the same as panel (a) but for the respective maximum cloud areas before and after an EMT vacate the TP. Panel (d) is the same as panel (b), but for the respective standardized time before and after an EMT vacate the TP. AEMT, after an EMT move off the TP; BEMT, before an EMT move off the TP

Figure 11b shows the STs when the EMTs and NDTs have their maximum cloud areas in each month. In May, the medians STs of the EMTs and NDTs are both around 0.65; this means that their maximum cloud areas generally appear in similar stages, namely the latter half of their lifespans. By contrast, during the other months, the EMT maximum cloud area generally appears earlier than the NDT one. Because the EMT maximum cloud area generally exceeds the NDT one (Figure 11a), the difference in ST at maximum cloud area means that EMTs develop more rapidly than do NDTs.

Similar to Equation (1), we define the time at which an EMT attains maximum area over the TP (resp. off the TP) divided by the time that is persists over the TP (resp. off the TP) as the ST for the EMT's maximum cloud area over the TP (resp. off the TP). As Figure 11d shows, in each month, the STs of the EMTs' maximum cloud areas over the TP generally exceed those when the EMTs are off the TP. The median of the former is 0.6–0.9, which means that the EMTs tend to attain their maximum cloud areas when they are about to vacate the TP. The median of the latter is around 0.5, which means that after the EMTs vacate the TP, they can generally develop again, with their maximum cloud areas appearing around halfway through the time that they persist off the TP.

After an EMT vacates the TP, one of four scenarios ensue: (a) it dissipates rapidly; (b) it dissipates gradually with increasing TBB but increasing area; (c) it develops initially and then dissipates; (d) it merges with local MCSs, causing its area to grow appreciably. As Figure 12 shows, the maximum cloud areas of EMTs tend to appear around the eastern flank of the TP (i.e., 101–104°E). Overall, during the warm season, more than 60% of EMTs maximize their cloud areas over the TP (Figure 12f), although the monthly proportions differ considerably. In July and August, around 70% of EMTs reach their maximum cloud areas over the TP, whereas in May more than half (~52%) of the EMTs attain their maximum cloud areas after they vacate the TP.

From Figure 13a,b, the maximum AGRs of EMTs generally exceed those of NDTs and also appear earlier; this means that compared to NDTs, EMTs develop more rapidly and reach maturity earlier. When EMTs are over the TP, their maximum AGRs generally exceed those after they vacate the TP (Figure 13c); this means that after an EMT vacates the TP it develops less rapidly. From Figure 5b,d, EMTs generally have lower mean minimum TBBs and larger mean maximum TBB gradients when they are over the TP than once they have vacated the TP; this also means that EMTs tend to weaken after they vacate the TP.

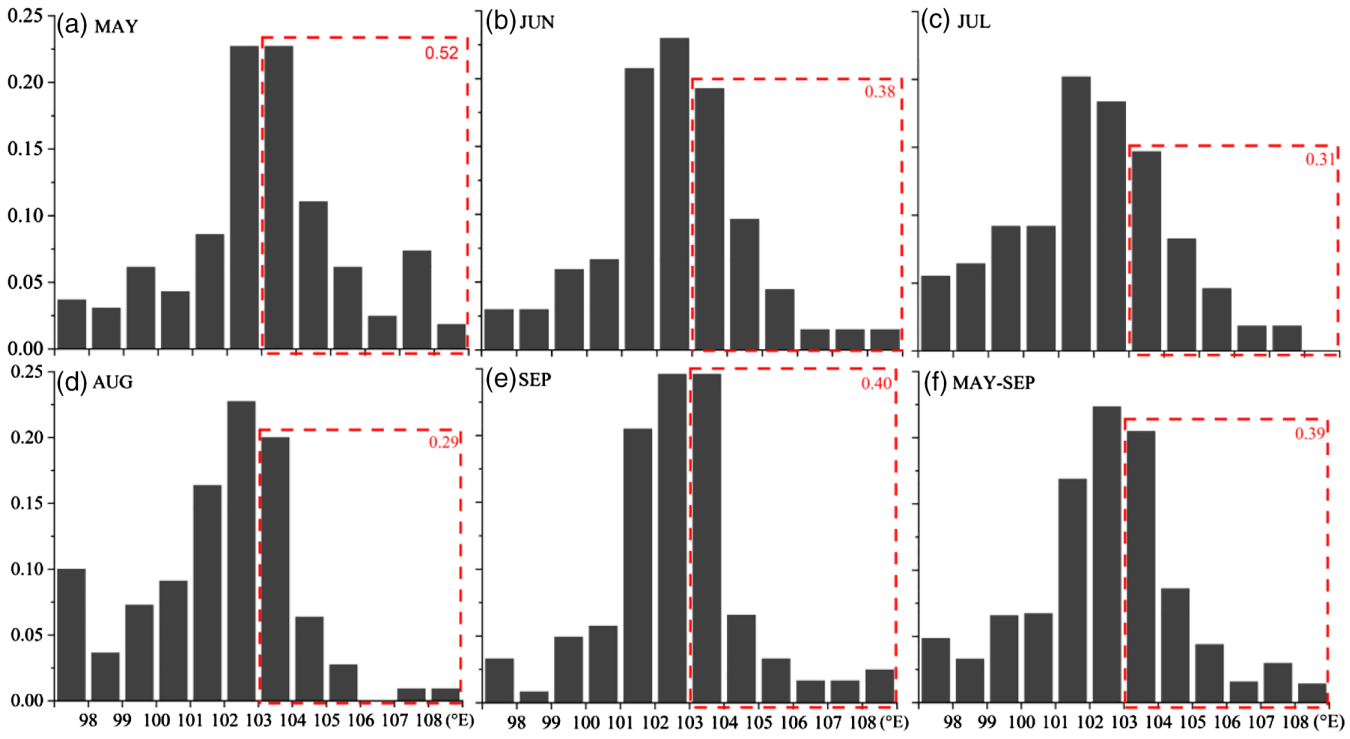

FIGURE 12 The ratio of numbers of EMTs that reach maximum cloud area at each longitude to the total EMT numbers during each month and the warm season, where the red rectangle marks the accumulated ratio in regions east of 103°E

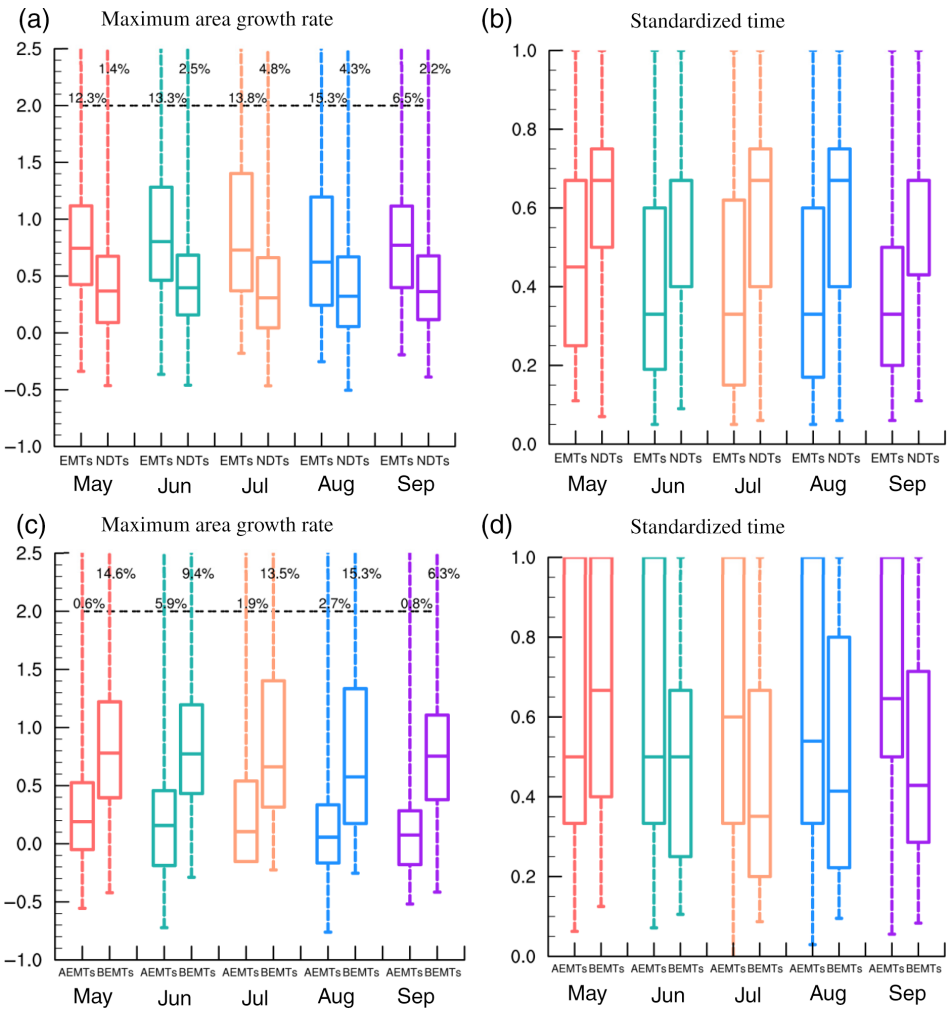

FIGURE 13 The same as Figure 11, but for maximum area-growth rate

Comparing the ST medians in Figures 11d and 13d, it can be seen that, over the TP, the average median ST for maximum cloud area during the study period exceeds that for maximum AGR, which indicates that EMTs generally first attain their maximum AGRs and then attain their maximum cloud areas over the TP. By contrast, after EMTs vacate the TP, the average median ST for maximum cloud area is smaller than that for maximum AGR, so they generally first attain their maximum cloud areas and then attain their maximum AGR. This means that after vacating the TP, EMTs tend to weaken initially and then develop again. Generally, the maximum AGRs appear halfway through the time of persistence off the TP (Figure 13d).

4 | COMPOSITE FEATURES

In this study, we investigate the composite of EMTs and NDTs to show their respective key features and main differences. We begin by interpolating the six-hourly CFSR data linearly into three-hourly resolution. Based on this 3-hourly dataset, we composite the EMTs/NDTs during their lifespans in the Euler coordinate to focus on their environmental circulations. In addition, we composite the L-EMTs during their typical stages in the Lagrange coordinate (i.e., the coordinate centered in the MCS' centers) to focus on their evolution.

4.1 | Overall environmental features of the EMTs and NDTs

For the EMTs, in the upper troposphere, their highly frequent occurrence regions (Figure 7e) are mainly located northeast of a weak South Asian high (where divergence appears) and south of an upper-level jet core (Figure 14a). The upper-level divergence contributes to EMTs' formation/development, and the westerly wind around the eastern TP favours their eastward displacement. In the middle troposphere, the active regions of EMTs (Figure 7e) are under the influences of a shallow shortwave trough over the eastern TP (Figure 14b). Around this active region, the air is moist. This favours the condensation-related latent heating that is conducive to convection

intensification. A comparison between Figures 7e and 14b indicates that, the active regions for EMTs have a different distribution from that of the moisture. In the lower troposphere, a stronger cyclonic circulation (compared to that of NDTs; cf., Figure 14c,f) with abundant moisture appears around the Sichuan Basin (Figure 14c). This

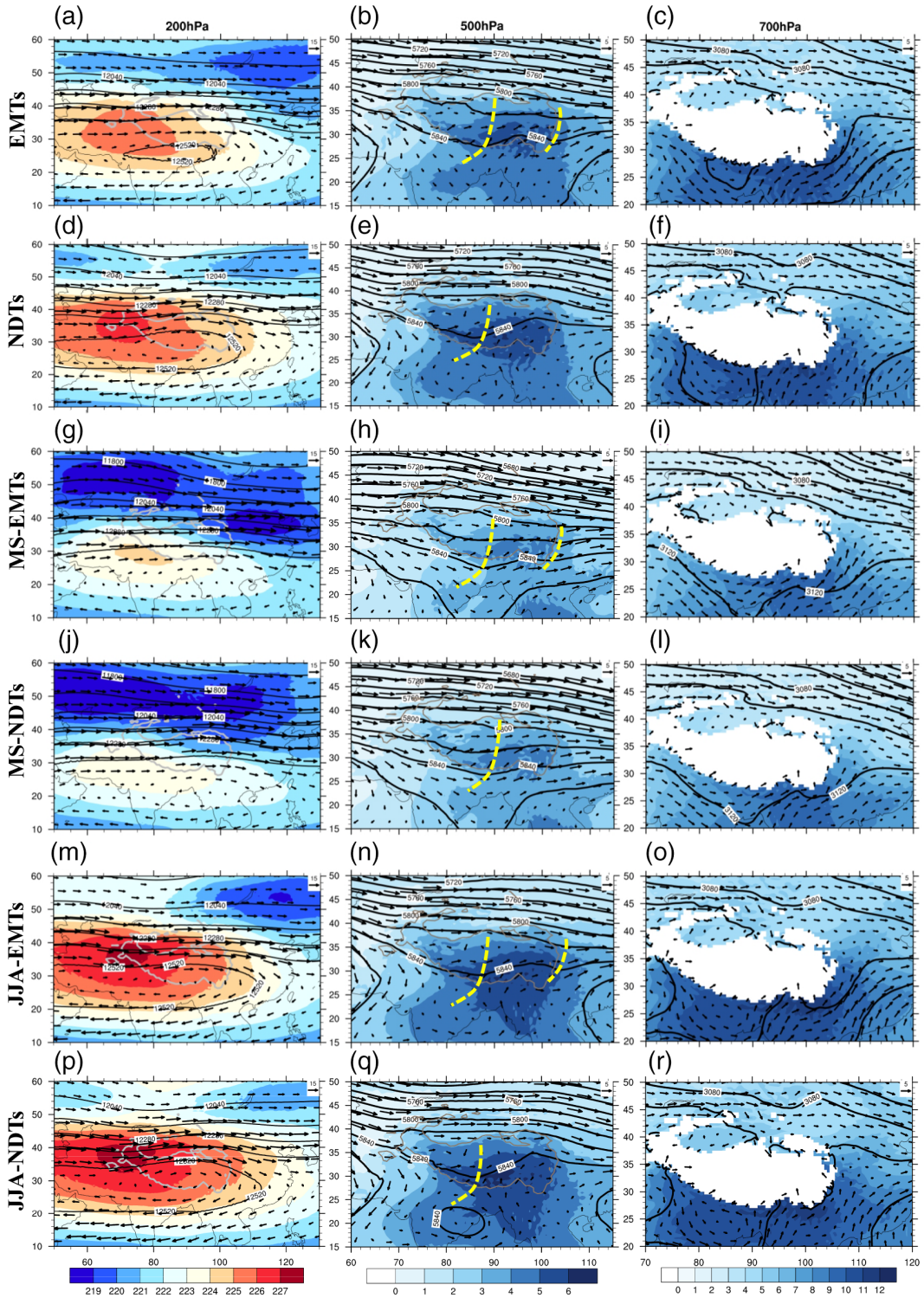

FIGURE 14 Composite (in Euler coordinate) geopotential height (black lines, units: gpm) and wind filed (vector, units: m s^{-1}) at 200 hPa (left column), 500 hPa (middle column), and 700 hPa (right column) of EMTs (a–c), NDTs (d–f), EMTs in May and September (MS) (g–i), NDTs in MS (j–l), EMTs in June July and August (JJA) (m–o), and NDTs in JJA (p–r), respectively, where shading in the left column is temperature (units: K), and in other columns it is specific humidity (units: g kg^{-1}). Grey lines and the white shading outline the topography of 3,000 m, and the yellow dashed lines are trough lines

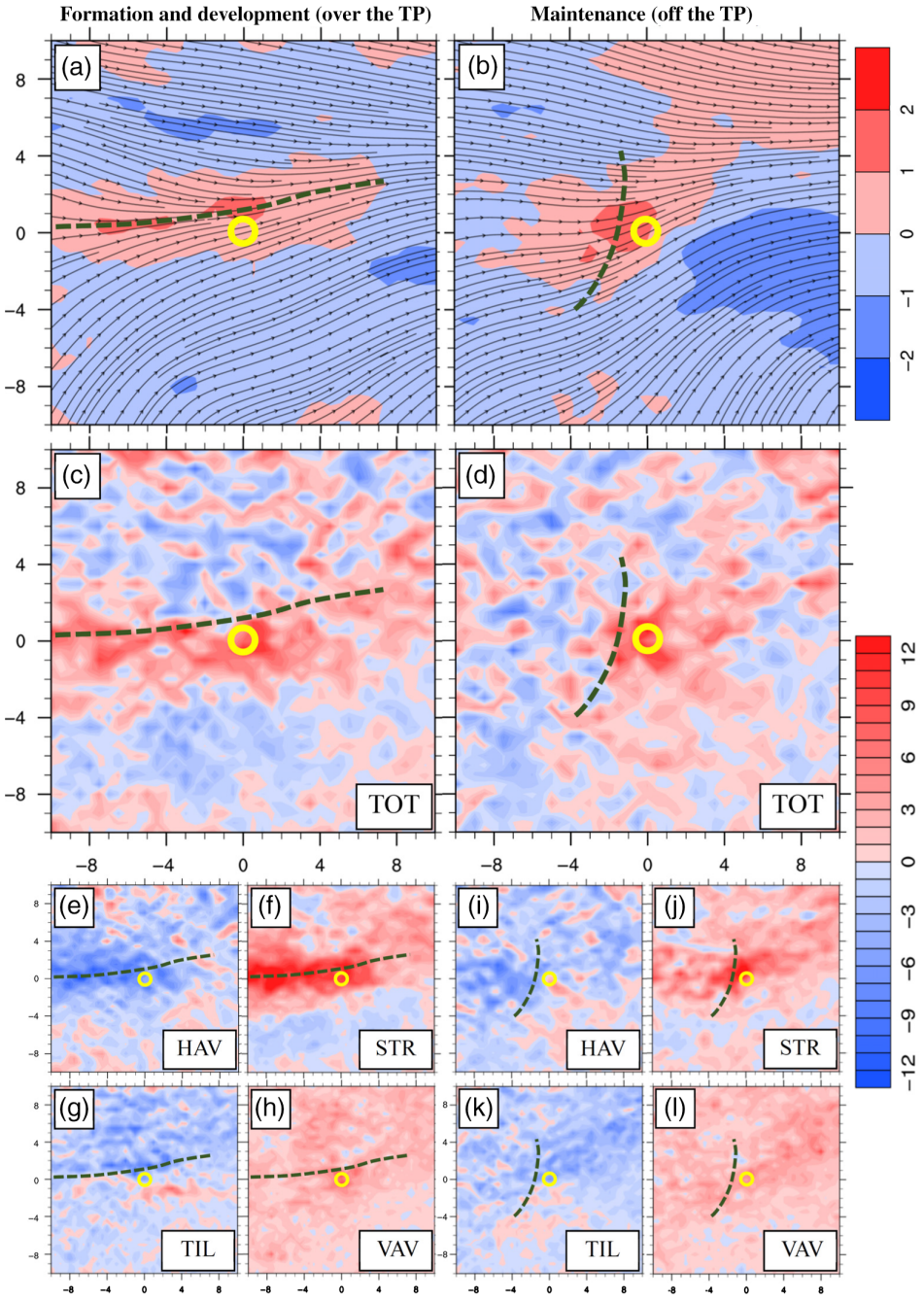

FIGURE 15 Composite (in Lagrange coordinate) of vorticity (shading, units: 10^{-5} s^{-1}) and stream field at 500 hPa for L-EMTs during the formation and development stage (a) and the maintenance stage (b). Term TOT at 500 hPa (shading, units: 10^{-9} s^{-2}) for L-EMTs during the formation and development stage (c) and maintenance stage (d). Panels (e–h) show the vorticity budget terms HAV, STR, TIL, and VAV (shading, units: 10^{-9} s^{-2}) at 500 hPa for L-EMTs during the formation and development stage. Panels (i–l) are the same as (e–h), but for the maintenance stage. The green dashed lines are the convergent line and trough line at 500 hPa and the yellow circle marks the center of the composite MCS

contributes to the maintenance of EMTs after they vacate the TP.

For the NDTs, their highly frequent occurrence regions (Figure 7f) are mainly located within the northeastern section of a strong South Asian high in the upper troposphere (Figure 14d), and ahead of a shortwave trough around 85°E in the middle troposphere (Figure 14e). This configuration provides upper-level divergence and favourable middle-level quasi-geostrophic forcings (associated with the warm temperature advection and cyclonic vorticity advection), both of which promote ascending motions (Holton, 2004). The active regions for NDTs are consistent with the distribution of moisture (cf., Figures 7f and 14e). Within these active regions, the westerly wind component is weak. This is a possible reason for why NDTs do not vacate the TP from its eastern boundary.

4.2 | Contrasts of EMTs and NDTs in the environmental features

The EMTs and NDTs differ remarkably from each other in their environmental circulations (Figure 14a–f). These

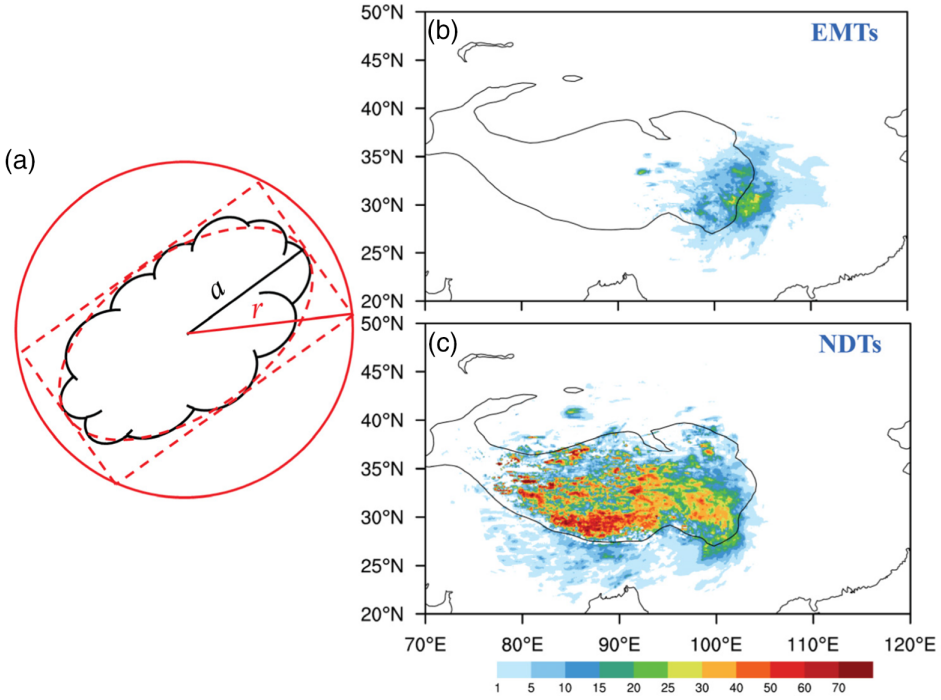

FIGURE 16 Panel (a) is the schematic illustration of how calculate the precipitation related to an MCS, where *a* is the semi-major axis of the MCS, the ellipse outlines main body of the MCS, the big red circle marks the range within which the precipitation is related to this MCS, and *r* is the radius of this red circle. Panel (b) indicates the contribution of EMT-related precipitation to the local total accumulated precipitation during the warm season (shading, units: %). Panel (c) is the same as (b), but for NDT-related precipitation

differences are closely related to the seasonal variations of the weather systems around the TP (Hu *et al*., 2016). In order to remove the seasonal variations, the EMTs/NDTs are composited in May and September (MS) (i.e., the drier seasons), and June, July and August (JJA) (the moister seasons), respectively. In the upper troposphere, the most notable difference during MS is that the zonal temperature gradient is larger for the EMTs (cf., Figure 14g,j). This results in stronger warm temperature advection for the EMTs, which contributes to convection through inducing pressure lowering (Markowski and Richardson, 2010). During JJA, the South Asian high is stronger for the NDTs (cf., Figure 14m,p), but the westerly wind over the eastern TP is stronger for the EMTs, which is conducive to their eastward displacement. In the middle troposphere, for both MS and JJA, or even the whole warm season, the main differences between EMTs and NDTs include: (a) a shallow trough appears over the eastern TP for the EMTs (the middle column of Figure 14), which means the dynamical conditions (Holton, 2004) are better for EMTs; and (b) moisture is more abundant for NDTs. The active regions for NDTs have similar distributions to that of the moisture (cf., Figures 7f and 14e,k,q). This contrasts to the situation of the EMTs (cf., Figures 7e and 14b,h,n). During JJA, the westerly wind over the eastern TP is stronger for the EMTs (cf., Figure 14n,q), which favours its eastward movement. In the lower troposphere, around the Sichuan Basin, geopotential height is lower for the EMTs during both MS (cf., Figure 14i,l) and JJA (cf., Figure 14o,r), and the moisture is more abundant for EMTs. These contribute to maintenance of EMTs after they vacate the TP.

4.3 | Composite of L-EMTs

As the L-EMTs have longest life spans and largest impacts on the downstream regions, we composite them in the Lagrange coordinate (i.e., use the coordinate centered in the center of each L-EMT) to investigate their evolution. Two typical stages are used in the composite: (a) from 3-hr before the formation of each L-EMT to 3-hr after its formation, which is used to mainly focus on its formation and development; and (b) the lifespans after the L-EMT has vacated the TP, which is used to mainly focus on its maintenance off the TP. As Figure 15a,b show, during the formation and development stage, L-EMTs are associated with a convergent line over the TP, whereas during the maintenance stage, L-EMTs are associated with a shallow trough east of the TP. Both of the aforementioned convergent line and trough feature notable cyclonic vorticity, which can reflect the variation of the L-EMTs effectively (Markowski and Richardson, 2010; Fu *et al*., 2011). The vorticity budget (section 2d) is used to understand the mechanisms underlying the L-EMTs' variation. From Figure 15c,d, dynamical conditions are mainly conducive to the L-EMTs' formation, development, and maintenance, particularly in the regions south of the convergent line and east of the shallow trough, because the total effect of the vorticity budget (i.e., TOT) is positive.

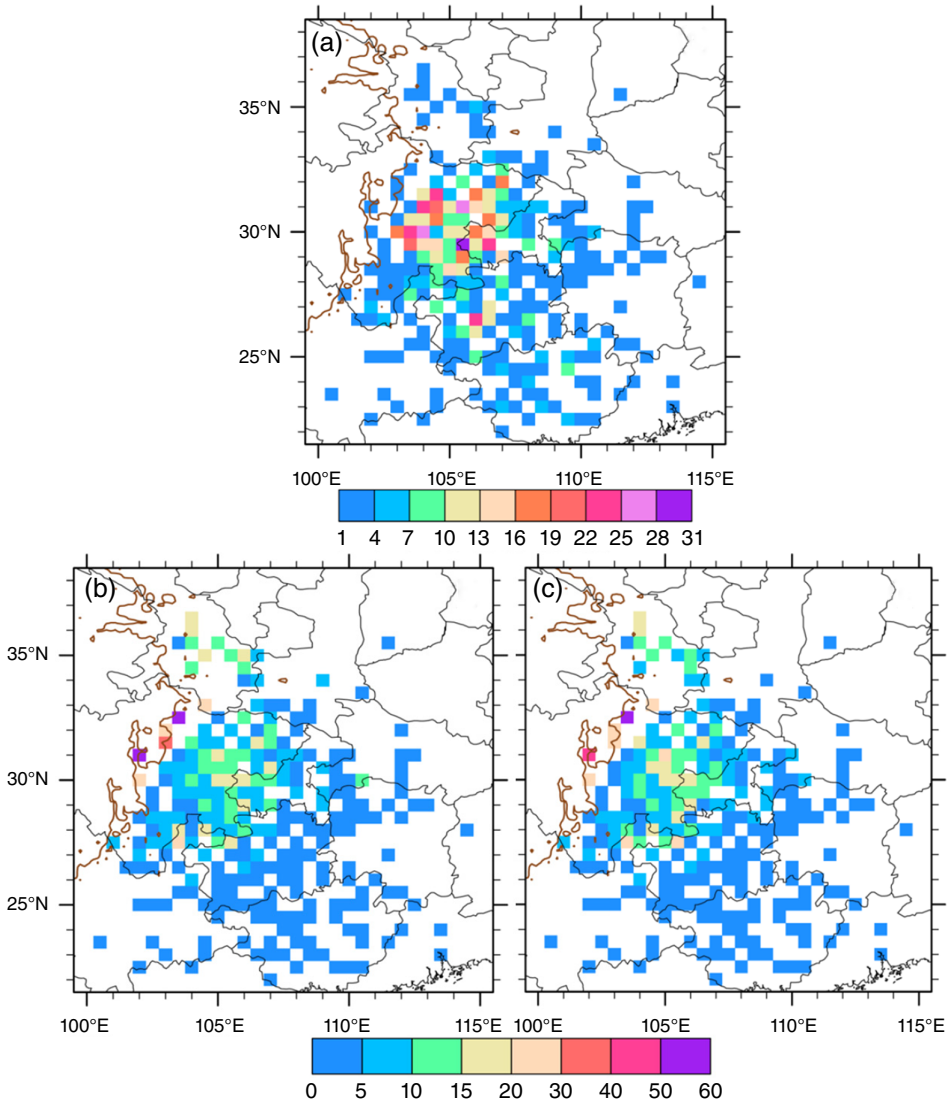

FIGURE 17 Panel (a) shows the distribution and total number of hourly heavy precipitation events that are related to EMTs. Panel (b) shows the contribution of EMT-related hourly heavy precipitation to the total numbers of hourly heavy precipitation during the study period (units: %). Panel (c) is the same as (b), but for the contribution of accumulated precipitation

For the formation and development stage, the convergence-related horizontal shrinking (i.e., STR) (Figure 15f) and convection-related vertical transport of vorticity (i.e., VAV) (Figure 15h) act as the most and second most favourable factors for the L-EMTs' formation and development. In contrast, the horizontal transport (i.e., HAV) (Figure 15e) and tilting (i.e., TIL) (Figure 15g) serve as the most and second most detrimental factors. For the maintenance stage off the TP, the convergence-related horizontal shrinking (Figure 15j) and convection-related vertical transport of vorticity (Figure 15l) still act as the favourable factors, whereas, the relative importance of STR reduces, as the convergence associated with the L-EMTs weakens after they vacate the TP. There are three main reasons for the weakening of convergence and its associated STR: (a) intrinsic difference appears in the cyclonic circulations associated with L-EMTs before and after they vacating the TP; (b) the direct sensible heating from the TP surface on the bottom of the L-EMTs disappears; and (c) convective ascending motions associated with the L-EMTs weakens (according to fluid continuity, convergence will decrease) as the increasing of TBB shows (Figure 5d). The horizontal transport (Figure 15i) and tilting (Figure 15k) show similar contributions in decelerating the cyclonic-vorticity maintenance associated with the L-EMTs. This is different from the situation during the formation and development stage.

5 | CONTRIBUTION OF MCS-RELATED PRECIPITATION

In this study, we calculate the contributions of MCS-related precipitation to the total accumulated precipitation during the warm season. Rather than using the three-hourly $0.25^\circ \times 0.25^\circ$ TRMM_3B42 precipitation data (Turk and Miller, 2005; Turk *et al.*, 2010), we use the CMORPH data (30-min temporal resolution and 8-km

TABLE 2 Key characteristics of EMTs that are related to SWVs

	AFL	AMTT	AMTO	ALSE	ASTM
EMTs related to SWVs	100.1	8.7	17.6	26.3	0.41
EMTs related to SWV formation	100.2	8.7	18.5	27.2	0.40
MCSs related to SWVs (excluding SWV formation)	99.9	9.2	10.7	19.8	0.51

Abbreviations: AFL, averaged formation longitude; ALSE, averaged lifespans of EMTs (units: hours); AMTO, averaged maintaining time off the TP (units: hours); AMTT, averaged maintaining time over the TP (units: hours); ASTM, averaged standardized time when EMTs vacate the TP.

spatial resolution) (Joyce *et al.*, 2004) to evaluate the contribution of MCSs to precipitation, for the CMORPH data are easily to interpolate into 1-hr temporal resolution, which is consistent to the temporal resolution of TBB. Results documented in Shen *et al.* (2010; 2014) show the CMORPH data can provide credible precipitation estimate in China. Although Huang *et al.* (2016) suggest that CMORPH precipitation may underestimate the precipitation over the TP, Blamey and Reason (2013) point out that this possible underestimate is not important for a study focused on evaluating the precipitation contribution.

Using the method documented by Ai *et al.* (2016), we estimate the hourly precipitation of each MCS based on the parameters obtained by the tracking algorithm. We determine the precipitation related to an MCS as follows. The tracking algorithm identifies the outline of an MCS as a closed curve (Figure 16a), based on which an ellipse and its long/short axis can be determined. Using the long and short axes, a rectangle tangent to the ellipse can be drawn. Using the diagonal of this rectangle (using the radius r), a large circle can be determined. The hourly precipitation within this large circle during the focus period is considered to be related to this MCS. By calculating the precipitation of all MCSs at a same hour and eliminating the repeated calculation of precipitation among adjacent MCSs, we estimate the hourly precipitation related to MCSs. After that, we accumulate the hourly MCS-related precipitation at all grids within the tracking range during all the warm seasons. The resulted value is then divided by the total accumulated precipitation within the same range and during the same period. This produces a ratio, which can be regarded as the contribution of MCS-related precipitation to the total local precipitation.

As Figure 16c shows, precipitation related to NDTs accounts for a significant proportion of the total precipitation over the TP. For the two active centers of NDTs shown in Figure 6f, the NDT-related precipitation accounts for contributions up to 70% (Figure 16c). In addition, some regions over the northern and central TP are also affected significantly by the NDT-related precipitation, with a contribution of around 60%. Compared to NDTs, EMTs generally make a much smaller contribution to local precipitation because there are far fewer EMTs than NDTs. However, for some regions such as the TP's eastern flank and the Sichuan Basin, the EMT-related precipitation can also make a notable contribution (~50% to that due to NDTs) to the local total precipitation. Considering in these regions NDTs' number is much larger than that of EMTs (~3 times), it can be concluded that around the eastern flank of the TP and the Sichuan Basin, the EMT-related precipitation is more intense than that related to NDTs.

The EMT-related precipitation is important to downstream regions east of the TP (but west of 110°E), particularly for the regions around the Sichuan Basin (Figure 16b), where heavy rainfall (according to CMA, if the hourly accumulated precipitation of an event is above 20 mm, it is an hourly heavy rainfall) and associated disasters occurs frequently. This study uses the hourly precipitation observational data from CMA and the method shown in Figure 16a to determine the EMT-related hourly heavy precipitation. After EMTs vacate the TP, they show close relationship to hourly heavy precipitation events in the downstream regions (Figure 17a), particularly around the Sichuan Basin and Guizhou Province. Since Sichuan Basin and Guizhou Province are mainly affected by eastward and southeastward moving EMTs, the distribution in Figure 17a also means that the eastward- and southeastward-moving EMTs are more closely related to hourly heavy precipitation events (than are northeastward-moving EMTs). As Figure 17b,c show, the EMT-related hourly heavy precipitation makes a contribution of 10–20% to the total number and total accumulated precipitation of hourly heavy precipitation events around the Sichuan Basin and southern Gansu Province. In contrast, for the other regions, the contribution from EMT-related hourly heavy precipitation is generally below 10%.

6 | RELATIONSHIP BETWEEN EMTS AND SWVS

Previous studies (Lu, 1986; Fu *et al.*, 2011) find that for some MCSs, after they moving out from the TP, they can induce SWVs around Sichuan Basin. The SWVs frequently induce

heavy rainfall east of the TP. In the present study, we conduct a statistical analysis on the SWVs related to the EMTs. The analysis is conducted using the three-hourly 0.5° × 0.5° CFSR data (we interpolate linearly the original six-hourly temporal resolution to 3-hourly), during the whole study period. This standard for detecting an SWV is the same as that documented by Fu *et al.* (2015): a meso-α scale (Orlanski, 1975) cyclonic closed-stream center coupled with a remarkable positive vorticity center appearing at 700 hPa, the central level of SWVs (Fu *et al.*, 2015). Depending on the time that elapses between an EMT and an SWV, there are two main scenarios: (a) if no SWV exists when the EMT begins to vacate the TP but one forms in the subsequent hours and the overlapping area between the EMT and SWV exceeds 20% of the EMT's area, then the EMT is considered to be related to the SWV formation; (b) if an SWV already exists when the EMT begins to vacate the TP and the overlapping area exceeds 20%, then the EMT is considered only to be associated with the SWV rather than with its formation. In the present study, events that do not satisfy a or b are deemed EMTs that are not related to SWVs.

The statistical results indicate that SWVs are closely related to EMTs, with the L-EMTs accounting for an overwhelming proportion, while a large majority of S-EMTs are not related to SWVs due to their rapid dissipation after vacating the TP. In total, 50 L-EMTs are associated with SWVs (i.e., satisfy I or II above), accounting for ∼15.9% of all L-EMTs. Among them, 44 L-EMTs are related to SWV formation, accounting for ∼14% of all L-EMTs and ∼88% of the EMTs that are associated with SWVs. For the EMTs that are related to SWVs but not to SWV formation, ∼83.3% of the SWVs enhance after the EMTs move out from the TP. For the EMTs that are related to SWV formation, ∼65.9% of the SWVs form within 9 hr after the EMTs have vacated the TP, whereas, only ∼13.6% of the SWVs form after 12 hr after the EMTs have moved off the TP. From Table 2, EMTs that are related to SWVs have much longer lifespans than the mean EMT lifespan. These EMTs spend more time off the TP than over it. Compared to the EMTs that are related to SWVs but not to SWV formation, the average formation location of EMTs that are related to SWV formation is at a larger longitude and their lifespans tend to be longer. They also tend to stay over the TP for less time, vacate it earlier, and persist for longer thereafter.

7 | DISCUSSION AND CONCLUSIONS

Based on the hourly satellite TBB data, MCSs that were generated over the TP during 16 warm seasons were investigated statistically in this study. By including more-recent satellite observational data in the analyses and focusing on a longer study period, the present study complements previous related research well. Moreover, by analysing additional key features of the MCSs, some new findings were obtained.

During the 16 warm seasons, 9,754 MCSs formed over the TP. These MCSs could appear anywhere over the TP, with two maximum frequency centers appearing in the southwestern and southeastern TP, respectively, corresponding to the moist regions ahead of a middle-tropospheric shortwave trough. Within these two centers, MCS-related precipitation contributed as much as approximately 70% of the total local precipitation, consistent with Li *et al.* (2008). The numbers of MCSs that were generated over the TP varied every warm season, from 445 in 2015 to 798 in 2016. However, in the whole study period, neither the occurrence numbers of these MCSs nor their other key characteristics (e.g., life spans, proportion of EMTs) were found to have a significant trend of increasing/decreasing. This contrasts to the significant warming trend (∼0.25°C/decade) of the surface temperature of the TP from 1998 to 2013 (Duan and Xiao, 2015).

The MCSs generated over the TP were classified as either EMTs or NDTs, which showed significantly different characteristics. On average, 572 NDTs formed over the TP per warm season; they could appear anywhere over the TP but their maximum frequency centers were located mainly over the southern TP. By contrast, only around 40 EMTs formed over the TP every warm season and were located mainly over the eastern flank of the TP. The MCSs that formed west of 90°E usually did not vacate the TP. The EMTs did not occur frequently in warm seasons, but their mean lifespan was more than twice that of all MCSs. Eastward-moving EMTs accounted for the largest proportion of all EMTs (∼78.3%). The influences of EMTs on precipitation were limited mainly to the range of 22–37°N, 100–115°E, with the regions around Sichuan Basin being affected most significantly. The EMTs contributed 10–20% of the hourly heavy precipitation events both in frequency and amount within this region.

In this study, the proportion of EMTs to all the MCSs over TP is much smaller, which is only ∼6.6%, compared to ∼47% in Li *et al.* (2008) and ∼49% in Hu *et al.* (2016). The average lifespan of MCSs in this study is also much smaller. In Li *et al.* (2008), the average convective system life cycle is about 36 hr; in Hu *et al.* (2016), most Tibetan convective systems' periods (>91%) in the TP are shorter than 24 hr and reach its peak at 12 hr, while in our study, the mean lifespan is about 6 hr. There are three main reasons for these differences: (a) compared to the 3-hourly (or coarser temporal resolution) dataset used in the

earlier studies, hourly TBB data are used in this study. This can effectively remove wrongly prolonged MCSs' life spans due to a coarse temporal resolution (many convections' lifespans are less than 3 hr); (b) according to Bluestein (1992), MCSs with larger horizontal scale tend to have longer time scale. For instance, in Hu *et al*. (2016), a convective system is defined as adjacent cloud clusters with an area $\geq 25 \times 10^3$ km^2, while the corresponding standard in this study is $\geq 5 \times 10^3$ km^2. (c) due to (a) and (b), MCSs' mean life spans are shortened. It is found that, around 75% of all NDTs lasted for less than 6 hr (Figure 3). It is hard for these MCSs ($\leqq$6 hr) to vacate the TP during such a short time. Therefore, the proportion of EMTs to all MCSs that generated over the TP is much less than those documented in previous studies.

Some entirely new findings of this study are also showed as follows:

1. Based on the hourly TBB data, through defining various parameters of the MCSs, key evolutionary characteristics of different types of MCSs are shown. Particularly, the key features before and after the MCSs vacating the TP, and the main changes during the vacating stage are illustrated. Overall, the EMTs had larger cloud areas, stronger intensities, more-rapid development, and longer lifespans, but made lower contributions to the local total precipitation. Usually, the EMTs began to vacate the TP in the latter half of their lifespans, tending to attain their maximum cloud areas when they were about to vacate the TP. After vacating the TP, the EMT trend was to weaken initially and then develop again. Generally, their most-rapid development off the TP tended to appear around halfway through the time for which they persisted off the TP.
2. The environmental circulations associated with EMTs and NDTs differed from each other remarkably. Overall, the upper-level divergence and middle-level moisture were more favourable for the NDTs, whereas, the middle-to-upper-level steering flow, the dynamical conditions related to the 500-hPa shallow trough over the eastern TP, as well as the 700-hPa cyclonic wind field, lower geopotential height, and more abundant moisture around the Sichuan Basin were more conducive for the EMTs. Vorticity budget showed that the convergence-related horizontal shrinking and the convection-related vertical vorticity transport dominated the cyclonic-vorticity increase/maintenance associated with the longer-lived EMTs.
3. the relationship between EMTs and SWVs are quantitatively estimated. During the study period, only ~8% of all EMTs were associated with SWVs, of which ~88% were related to SWV formation. It is found that, ~65.9% of the SWVs formed within 9 hr after the EMTs had vacated the TP. Compared to the mean for all EMTs, those EMTs that were related to SWVs usually remained over the TP for less time, vacated it earlier, persisted for longer thereafter, and had longer total lifespans.

ACKNOWLEDGEMENTS

The authors thank the NCEP, CMA, and JMA for providing the data. Sincere thanks are also extended to Dr Jun Li for his automatic tracking algorithm. This research was supported by the National Key R&D Program of China (2018YFC1507606), National Natural Science Foundation of China (grant nos. 91637211, 41775046, and 4157505), and the Youth Innovation Promotion Association of the Chinese Academy of Sciences.

ORCID

Shen-Ming Fu https://orcid.org/0000-0001-9670-0607

REFERENCES

Ai, Y., Li, W., Meng, Z. and Li, J. (2016) Life cycle characteristics of MCSs in middle East China tracked by geostationary satellite and precipitation estimates. *Monthly Weather Review*, 144, 2517–2530.

Augustine, J. and Howard, K. (1991) Mesoscale convective complexes over the United States during 1986 and 1987. *Monthly Weather Review*, 119, 1575–1589.

Blamey, R.C. and Reason, C.J.C. (2013) The role of mesoscale convective complexes in southern Africa summer rainfall. *Journal of Climate*, 26, 1654–1668.

Bluestein, H.B. (1992) *Synoptic-Dynamic Meteorology in Midlatitudes, Volume I, Principles of Kinematics and Dynamics*. Oxford: Oxford University Press, pp. 5–7.

Chen, L., Song, Y., Liu, J. and Wang, W. (1999) On the diurnal variation of convective over Qinghai-Xizang Plateau during summer as revealed from meteorological satellite data [in Chinese]. *Acta Meteorologica Sinica*, 57, 549–560.

Dai, X., Guo, Z., Wu, J., Li, W. and Lin, H. (2007) Clustering analysis of the feature of environmental physical field around the MCS moving eastward out of the Tibetan plateau in summer 1998 [in Chinese]. *Plateau Meteorology*, 26, 701–707.

Duan, A. and Xiao, Z. (2015) Does the climate warming hiatus exist over the Tibetan Plateau? *Scientific Reports*, 5, 13711.

Feng, Z., Dong, X., Xi, B., McFarlane, S.A., Kennedy, A., Lin, B. and Minnis, P. (2012) Life cycle of midlatitude deep convective systems in a Lagrangian framework. *Journal of Geophysical Research*, 117, D23201.

Flohn, H. and Reiter, E.R. (1968) Contributions to a meteorology of the Tibetan Highlands. *Atmospheric Science Papers*, 130.

Fu, S.-M., Sun, J.-H., Zhao, S.-X. and Li, W.-L. (2010) The impact of eastward propagation of convective systems over the Tibetan Plateau on southwest vortex formation in summer. *Atmospheric and Oceanic Science Letters*, 3, 51–57.

Fu, S.-M., Sun, J., Zhao, S., Li, W. and Li, B. (2011) A study of the impacts of the eastward propagation of convective cloud systems over the Tibetan Plateau on the rainfall of the Yangtze-Huai River basin [in Chinese]. *Acta Meteorologica Sinica*, 69, 581–600.

Fu, S.-M., Li, W., Sun, J., Zhang, J. and Zhang, Y. (2015) Universal evolution mechanisms and energy conversion characteristics of long-lived mesoscale vortices over the Sichuan Basin. *Atmospheric Science Letters*, 16, 127–134.

Fu, S.-M., Sun, J.-H., Luo, Y.-L. and Zhang, Y.-C. (2017) Formation of long-lived summertime mesoscale vortices over central east China: semi-idealized simulations based on a 14-year vortex statistic. *Journal of the Atmospheric Sciences*, 74, 3955–3979.

Fu, S.-M., Mai, Z., Sun, J.-H., Li, W.-L., Ding, Y. and Wang, Y. (2019) Impacts of convective activity over the Tibetan Plateau on plateau vortex, southwest vortex, and downstream precipitation. *Journal of the Atmospheric Sciences*, 76, 3803–3830.

Holton, J.R. (2004) *An Introduction to Dynamic Meteorology*. San Diego, CA: Elsevier Academic Press.

Hu, M.K. (1962) Visual pattern recognition by moment invariant. *IEEE Transactions on Information Theory*, 28, 179–187.

Hu, L., Deng, D., Gao, S. and Xu, X. (2016) The seasonal variation of Tibetan convective systems: satellite observation. *Journal of Geophysical Research*, 121, 5512–5525.

Hu, L., Deng, D., Xu, X., Xu, X. and Zhao, P. (2017) The regional differences of Tibetan convective systems in boreal summer. *Journal of Geophysical Research*, 122, 7289–7299.

Huang, A., Zhao, Y., Zhou, Y., Yang, B., Zhang, L., Dong, X., Fang, D. and Wu, Y. (2016) Evaluation of multisatellite precipitation products by use of ground-based data over China. *Journal of Geophysical Research*, 121, 654–675.

Jiang, J. and Fan, M. (2002) Convective clouds and mesoscale convective systems over the Tibetan Plateau in summer [in Chinese]. *Chinese Journal of Atmospheric Sciences*, 26, 263–270.

Jiang, J., Xiang, X. and Fan, M. (1996) The spatial and temporal distributions of severe mesoscale convective systems over Tibetan Plateau in summer [in Chinese]. *Acta Meteorologica Sinica*, 4, 473–478.

Joyce, R.J., Janowiak, J.E., Arkin, P.A. and Xie, P. (2004) CMORPH: a method that produces global precipitation estimates from passive microwave and infrared data at high spatial and temporal resolution. *Journal of Hydrometeorology*, 5, 487–503.

Kondo, Y., Higuchi, A. and Nakamura, K. (2006) Small-scale cloud activity over the maritime continent and the western Pacific as revealed by satellite data. *Monthly Weather Review*, 134, 1581–1599.

Laing, A. and Fritsch, J. (1997) The global population of mesoscale convective complexes. *Quarterly Journal of the Royal Meteorological Society*, 123, 389–405.

Li, J. (2010) *Study on the Characteristics of the Mesoscale Convective Cloud Clusters Occurred in East Asia during Warm Seasons*. Beijing: [in Chinese]. Institute of Atmospheric Physics, Chinese Academy of Sciences, pp. 1–29.

Li, C., Wang, Z., Lin, S. and Gao, H. (2004) The relationship between East Asia summer monsoon activity and northward jump of the upper westerly jet location [in Chinese]. *Chinese Journal of Atmospheric Sciences*, 28, 641–658.

Li, Y., Wang, Y., Yang, S., Hu, L., Gao, S.T. and Fu, R. (2008) Characteristics of summer convective systems initiated from Tibetan Plateau part I: origin, track, development and precipitation. *Journal of Applied Meteorology and Climatology*, 47, 2679–2695.

Lu, J. (1986) *Generality of the Southwest Vortex* [in Chinse], Vol. 270 Beijing: China Meteorological Press.

Lu, X., Ma, J. and Wu, C. (1987) A shape analytical method of two dimensional objects [in Chinese]. *Journal on Communications*, 8, 61–67.

Maddox, R.A. (1980) Mesoscale convective complexes. *Bulletin of the American Meteorological Society*, 61, 1374–1387.

Markowski, P. and Richardson, Y. (2010) *Mesoscale Meteorology in Midlatitudes*. Hoboken, NJ: Wiley-Blackwell, p. 407.

Mathon, V. and Laurent, H. (2001) Life cycle of Sahelian mesoscale convective cloud systems. *Quarterly Journal of the Royal Meteorological Society*, 127, 377–406.

Murata, H., Takahashi, M. and Kosaka, Y. (2015) VIS and IR bands of Himawari-8/AHI compatible with those of MTSAT-2/imager. *Meteorological Satellite Center Technical Note*, 60, 1–18.

Orlanski. (1975) A rational subdivision of scales for atmospheric processes. *Bulletin of the American Meteorological Society*, 56, 527–530.

Parker, M.D. and Johnson, R.H. (2000) Organizational modes of midlatitude mesoscale convective systems. *Monthly Weather Review*, 128, 3413–3436.

Qian, Z., Zhang, S. and Shan, F. (1984) *Analysis on Summer Convection Cloud in Qinghai-Tibetan Plateau Area Corpus I about Meteorological Experiment on Qinghai-Tibatan Plateau*. Beijing: [in Chinese]. Science Press, pp. 243–245.

Qie, X., Wu, X., Yuan, T., Bian, J. and Lu, D. (2014) Comprehensive pattern of deep convective systems over the Tibetan Plateau-South Asian monsoon region based on TRMM data. *Journal of Climate*, 24, 6612–6626.

Saha, S., Nadiga, S., Thiaw, C., Wang, J., Wang, W., Zhang, Q., Van den Dool, H.M., Pan, H.-L., Moorthi, S., Behringer, D., Stokes, D., Peña, M., Lord, S., White, G., Ebisuzaki, W., Peng, P. and Xie, P. (2006) The NCEP climate forecast system. *Journal of Climate*, 19, 3483–3517.

Saha, S., Moorthi, S., Wu, X., Wang, J., Nadiga, S., Tripp, P., Behringer, D., Hou, Y.-T., Chuang, H.-y., Iredell, M., Ek, M., Meng, J., Yang, R., Mendez, M.P., van den Dool, H., Zhang, Q., Wang, W., Chen, M. and Becker, E. (2014) The NCEP climate forecast system version 2. *Journal of Climate*, 27, 2185–2208.

Shen, Y., Xiong, A., Wang, Y. and Xie, P. (2010) Performance of high-resolution satellite precipitation products over China. *Journal of Geophysical Research*, 115, D02114.

Shen, Y., Zhao, P., Pan, Y. and Yu, J. (2014) A high spatiotemporal gauge-satellite merged precipitation analysis over China. *Journal of Geophysical Research – Atmospheres*, 119, 3063–3075.

Sugimoto, S. and Ueno, K. (2010) Formation of mesoscale convective systems over the eastern Tibetan plateau affected by plateau-scale heating contrasts. *Journal of Geophysical Research*, 115, 3413–3436.

Tahara, Y. and Ohkawara, N. 2005 Status of MTSAT-1R and recent activities in MSC. In: *Proceedings of the 2005 EUMETSAT Meteorological Satellite Conference, 19–23 September 2005, Dubrovnik, Croatia*. EUMETSAT P., 46, pp. 9–15.

Tahara, Y., Ohkawara, N. and Okuyama, A. (2004) Intercalibration ofthe infrared channels between GMS-5 and GOES-9. *Meteorological Satellite Center Technical Note*, 44.

Turk, F.J. and Miller, S.D. (2005) Toward improved characterization of remotely sensed precipitation regimes with MODIS/AMSR-E blended data techniques. *IEEE Transactions on Geoscience and Remote Sensing*, 43, 1059–1069.

Turk, J.T., Mostovoy, G.V. and Anantharaj, V. (2010) The NRL-blend high resolution precipitation product and its application to land surface hydrology. In: *Satellite Rainfall Applications for Surface Hydrology*. Dordrecht: Springer, pp. 85–104.

Wang, W., Kuo, Y. and Warner, T. (1993) A diabatically driven mesoscale vortex in the lee of the Tibetan Plateau. *Monthly Weather Review*, 121, 2542–2561.

Xu, W. and Zipser, E.J. (2015) Diurnal variations of precipitation, deep convection, and lightning over and east of the eastern Tibetan Plateau. *Journal of Climate*, 24, 448–465.

Yang, W., Ye, D. and Xiong, G. (1992) The influence of the Tibetan Plateau on the thermal and circulation fields over east asia in summer II: main features of the local circulation fields and the large scale vertical circulation fields [in Chinese]. *Chinese Journal of Atmospheric Sciences*, 16, 287–301.

Yang, X., Fei, J., Huang, X., Cheng, X., Carvalho, L.M.V. and He, H. (2015) Characteristics of mesoscale convective systems over China and its vicinity using geostationary satellite FY2. *Journal of Climate*, 28, 4890–4907.

Yang, R.-Y, Zhang, Y.-C, Sun, J.-H, Fu, S.-M. & Li, J (2018) The characteristics and classification of eastward-propagating mesoscale convective systems generated over the second-step terrain in the Yangtze River Valley. *Atmos. Sci. Lett.*, 20:e874. https://doi.org/10.1002/asl.874.

Ye, D. and Gao, Y. (1979) *The Meteorology of Qinghai–Xizang (Tibet) Plateau* [in Chinese], Vol. 278 Beijing: Science Press.

Zhao, S., Tao, Z., Sun, J. and Bei, N. (2004) *Study on Mechanism of Formation and Development of Heavy Rainfalls on Meiyu Front in Yangtze River* [in Chinese], Vol. 282 Beijing: China Meteorological Press.

Zhao, P., Xu, X., Chen, F., Guo, X., Zheng, X., Liu, L., Hong, Y., Li, Y., La, Z., Peng, H., Zhong, L., Ma, Y., Tang, S., Liu, Y., Liu, H., Li, Y., Zhang, Q., Hu, Z., Sun, J., Zhang, S., Dong, L., Zhang, H., Zhao, Y., Yan, X., Xiao, A., Wan, W., Liu, Y., Chen, J., Liu, G., Zhaxi, Y. and Zhou, X. (2018) The third atmospheric scientific experiment for understanding the earth–atmosphere coupled system over the Tibetan Plateau and its effects. *Bulletin of the American Meteorological Society*, 99, 757–776.

Zheng, Y., Chen, J. and Jun, P. (2008) Climatological distribution and diurnal variation of mesoscale convective systems over China and its vicinity during summer. *Chinese Science Bulletin*, 53, 1574–1586.

Zhu, G. and Chen, S. (1999) Convective activities over the Qinghai-xizang plateau and adjacent regions in summer of 1995 [in Chinese]. *Plateau Meteorology*, 018(001), 9–19.

Zhuo, G., Xu, X. and Chen, L. (2002) Instability of eastward movement and development of convective cloud clusters over Tibetan Plateau [in Chinese]. *Journal of Applied Meteorology and Climatology*, 13, 448–456.

How to cite this article: Mai Z, Fu S-M, Sun J-H, Hu L, Wang X. Key statistical characteristics of the mesoscale convective systems generated over the Tibetan Plateau and their relationship to precipitation and southwest vortices. *Int J Climatol*. 2021;41 (Suppl. 1):E875–E896. https://doi.org/10.1002/joc.6735